

Microscopic theory for a minimal oscillator model of exciton-plasmon coupling in hybrids of 2d semiconductors and metal nanoparticles

Lara Greten,^{1,*} Robert Salzwedel,¹ Diana Schutsch,^{1,2} and Andreas Knorr^{1,†}

¹*Institut für Theoretische Physik, Technische Universität Berlin, Berlin, Germany*

²*Present address: Department of Engineering, Universitat Pompeu Fabra, Barcelona, Spain*

(Dated: October 23, 2024)

The common model to describe exciton-plasmon interaction phenomenologically is the coupled oscillator model. Originally developed for atomic systems rather than solid-state matter, this model treats both excitons and plasmons as single harmonic oscillators coupled via a constant which can be fitted to experiments. In this work, we present a modified coupled oscillator model specifically designed for exciton-plasmon interactions in hybrids composed of two-dimensional excitons, such as in a transition metal dichalcogenide (TMDC) monolayers and metal nanoparticles while maintaining the simplicity of the commonly applied coupled oscillator models. Our approach is based on a microscopic perspective and Maxwell's equations, allowing to analytically derive an effective exciton-plasmon coupling constant. Our findings highlight the importance of the spatial dispersion, i.e., the delocalized nature of TMDC excitons, necessitating the distinction between bright and momentum-dark excitons. Both types of excitons occur at different resonance energies and exhibit a qualitatively different coupling with localized plasmons. We find a strong coupling between the plasmon and momentum-dark excitons, while a weakly coupled bright exciton manifests as an additional, third peak in the spectrum. Consequently, we propose a realistic modeling of the primary spectral features in experiments incorporating three harmonic oscillator equations instead of the conventional two. However, we also shed light on the limitations of the three coupled oscillator model in describing the line shape of extinction and scattering cross section spectra.

I. INTRODUCTION

The concept of strong coupling between semiconductor or molecular excitons and localized plasmons in metal nanostructures has become increasingly important in the field of nanophotonics, as it offers a powerful way to control and manipulate light at the nanoscale [1]. Various realizations of exciton-plasmon hybrid systems exist, depending on the type of localized plasmons and excitons involved [2].

Localized surface plasmons (LSP) featured by metal nanoparticles (MNPs) or lattice modes, where arrays of metal nanostructures exhibit collective plasmonic modes [3, 4], allow for an extreme enhancement of the electric near-field and are promising for strong coupling with excitons up to room temperature [5–8].

For excitons, one distinguishes between two qualitatively different types: localized (0d) excitons, which occur in quantum dots [9] or molecules, e.g., J-aggregates [10, 11], and two-dimensional (2d) excitons, which are delocalized across extended two-dimensional semiconductors, such as mono- or few-layers of transition metal dichalcogenides (TMDCs). Due to the small thickness, atomically thin TMDCs exhibit high exciton binding energies thus offering stable excitonic spectral features even at room temperature. They are extremely sensitive to the environment and can be manipulated by their surrounding permittivity [12] or functionalization [13, 14], such as with plasmonic structures [15–18]. Moreover, the strong excitonic dipoles and pronounced light-matter interaction [19, 20] of TMDCs are of particular interest and, in this context, make them suitable for studying strong coupling phenomena in hybrid MNP-excitonic systems.

In addition to electric near-field exciton-plasmon coupling, which is the focus of this work, or Purcell-enhanced emission rates [21–23], e.g., for single photon generation [24–26], hybrid exciton-plasmon structures with direct electric contact [27, 28] are extensively studied regarding ultrafast charge transfer respectively hot electron injection [29, 30]. These can be used to manipulate optical and electronic properties via doping and are particularly relevant for applications in photo-induced catalysis [31].

Figure 1 sketches the hybrid system discussed in this work. It consists of a MNP on a two-dimensional TMDC monolayer substrate without direct electric contact. The MNP is modeled as a spheroid with semi-axes $r_x = r_y, r_z$ and permittivity

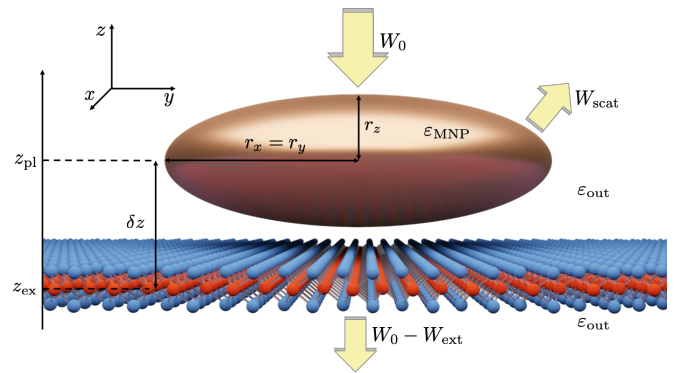


Figure 1. A gold nano-particle with half-axis r_x, r_y and r_z is located without direct contact on a TMDC monolayer with center-to-center distance $\delta z = |z_{\text{pl}} - z_{\text{ex}}|$ in a surrounding with permittivity ϵ_{out} . The electric field energy flow is illustrated with yellow arrows: the energy of the incident electric field (W_0), the scattering (W_{scat}) and the transmitted energy ($W_0 - W_{\text{ext}}$), that is, the incident energy minus the extinction (W_{ext}).

* lara.greten@tu-berlin.de

† andreas.knorr@tu-berlin.de

ϵ_{MNP} - we will use gold throughout this work - embedded in a surrounding with permittivity ϵ_{out} . The vertical separation between the MNP and the TMDC monolayer is denoted by the center-to-center distance $\delta z = |z_{\text{pl}} - z_{\text{ex}}|$. Figure 1 also illustrates the incident electric field respectively its associated energy flow W_0 and experimentally observable quantities such as extinction W_{ext} and scattering W_{scat} .

Since there is an increasing research interest in hybrid structures depicted in Fig. 1, models which are able to extract the coupling strength from experimental data are needed: Common models applied to hybrid systems are the coupled oscillator model (COM) [32–35], treating the exciton and plasmon each as a harmonic oscillator, or quantum mechanically the Jaynes-Cummings-model that represents the exciton as a two-level system in a single mode electric field [5, 36]. In these models, the coupling can be classified into different regimes. In the weak coupling regime, the interaction primarily enhances decay rates, such as the exciton’s radiative decay. In the strong coupling regime, when the coupling strength exceeds the decay rates, energy is coherently exchanged between the two modes over several oscillations, leading to the formation of new hybridized states, observable as an effective Rabi splitting in the spectrum [33]. More extreme regimes, such as ultra-strong [37] and deep-strong [38] coupling, involve even stronger interactions, where the coupling strength becomes a significant fraction of or comparable to the mode frequency. Since this leads to the breakdown of several approximations [39–41], we will not delve into these extreme regimes here.

When these models are applied to measurements of strong coupling for plasmonic structures interacting with localized (0d) excitons such as in Refs. [3, 5, 10, 42–45] or 2d TMDC excitons [6, 46–59], the coupling constant is treated as a fit parameter to categorize hybrid systems into a coupling regime. While this approach is useful for categorizing experimental data, it provides limited physical insight, particularly for the more complex behavior of 2d semiconductor excitons, which involve momentum-dark and bright states, typically not distinguished in phenomenological COMs. Computational simulations via Maxwell solvers are often applied [6, 47, 49, 53–57, 60, 61] for more quantitative predictions, but their quality depends on the applied excitonic model.

The goal of this paper is to propose an analytical, physically grounded model, which includes specifically important features of 2d excitons beyond a simple oscillator model. We aim to provide a model that can be easily applied to experimental data, while also offering a clear physical understanding of the underlying coupling mechanisms and incorporating key extensions to the COM to account for the spatial delocalization of the 2d excitons.

The paper is structured as follows: Section II provides a theoretical background on the optical properties of MNPs and two-dimensional excitons, e.g., in TMDC monolayers. It introduces the TMDC circular dichroism and, due to the delocalized nature of the 2d excitons, distinguishes between bright and momentum-dark excitons on the exciton dispersion. Starting from the microscopic exciton and plasmon dynamics, we derive in Sec. III a coupled harmonic oscillator model for the

exciton-plasmon interactions and provide formulas for typical, experimentally accessible observables. In this context, the section delves into the strongly different coupling character of bright and momentum-dark excitons to plasmons. We provide explicit microscopic parameters, which determine all coupling and dephasing constants in a COM combining three oscillators: plasmons, momentum-dark and bright excitons. In the results Sec. IV, we evaluate the observables under various conditions, demonstrating the sensitivity of the coupling strength on the exciton-plasmon distance, as well as to temperature and MNP packing density to highlight how the developed model differs from the conventional two coupled oscillator model.

II. OPTICAL PROPERTIES OF EXCITONS AND PLASMONS

In this section, we introduce excitons in TMDC monolayers via the excitonic Bloch equation [62] and discuss the distinction between bright and momentum-dark excitons. Next, we present the modeling of the optical near- and far-field response of plasmons in MNPs using Mie-Gans theory [63–65]. In both cases, we derive harmonic oscillator equations from the microscopic theory to approximately model their dynamics as driven by the incident electric field and occurring near-fields. MNP plasmon and the TMDC excitons are, if no electronic overlap (responsible for tunneling) exists, coupled via the total electric near-field [66] as the sum of the fields generated by exciton \mathbf{E}^{ex} , plasmon \mathbf{E}^{pl} and the incident electric field \mathbf{E}^0 :

$$\mathbf{E}(\mathbf{r}, \omega) = \mathbf{E}^{\text{ex}}(\mathbf{r}, \omega) + \mathbf{E}^{\text{pl}}(\mathbf{r}, \omega) + \mathbf{E}^0(\mathbf{r}, \omega) \quad (1)$$

All contributions in Eq. (1) are determined as a solution of Maxwell’s equations.

A. Excitons

The *Exciton Bloch Equation* for the dominant 1s excitonic transition $p_{\mathbf{q}_{\parallel}}^{\xi}$ with in-plane Fourier component \mathbf{q}_{\parallel} (also referred to as in-plane momentum) reads [13]

$$\left(\hbar\omega - \hbar\omega_{\text{ex}}(\mathbf{q}_{\parallel}) + \frac{i}{2}\hbar\gamma^{\text{ex}}(T) \right) p_{\mathbf{q}_{\parallel}}^{\xi}(\omega) = -\varphi_0^* \mathbf{d}^{\xi*} \cdot \mathbf{E}_{\mathbf{q}_{\parallel}}(\omega) \quad (2)$$

Equation (2) restricts to the lowest, 1s excitonic state, since it is energetically separated from higher excitonic transitions [67]. In Eq. (2), $\xi = K^+/K^-$ denotes the valley with direct band gaps, located at the corners of the first Brillouin zone of the electronic band structure. In the vicinity of the K^+/K^- valleys, the momentum-dependent exciton resonance frequency is described in parabolic approximation [68, 69]

$$\hbar\omega_{\text{ex}}(\mathbf{q}_{\parallel}) = \hbar\omega_{\text{ex}0} + \frac{\hbar^2 \mathbf{q}_{\parallel}^2}{2M}, \quad (3)$$

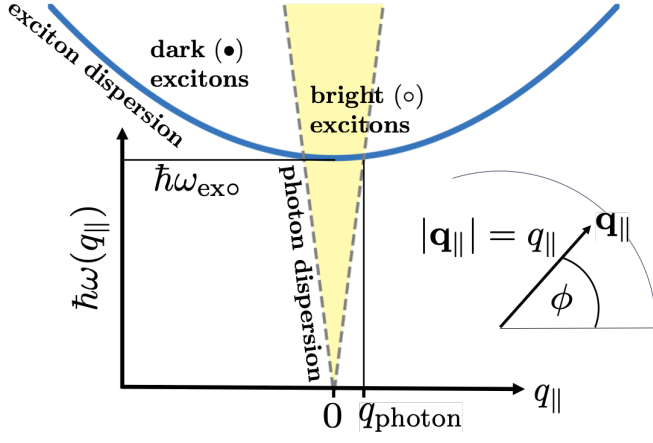


Figure 2. Sketch of the free exciton dispersion $\hbar\omega_{\text{ex}}(q_{\parallel})$ (blue). The light-cone, within the photon dispersion $\hbar\omega_{\text{photon}} = \frac{c}{\epsilon_{\text{out}}}q$, is shaded in yellow. Excitons in the light-cone ($q_{\parallel} < q_{\text{photon}}$) are bright (○). Excitons outside the light-cone ($q_{\parallel} > q_{\text{photon}}$) are momentum-dark (●). **inset:** 2d momentum \mathbf{q}_{\parallel} in polar representation with absolute value $|\mathbf{q}_{\parallel}| = q_{\parallel}$ and angle ϕ .

with the effective electron mass M parameterized from DFT calculations [70] and the resonance frequency ω_{exo} as observed in optical far-field spectroscopy. $\mathbf{q}_{\parallel} \approx 0$ corresponds to bright excitons, all other excitons are optically dark [71, 72]. Exciton and photon dispersions are schematically displayed in Fig. 2.

The temperature-dependent damping $\gamma^{\text{ex}}(T)$ in Eq. (2) accounts for non-radiative decay due to exciton-phonon interactions and is determined microscopically in Ref. 73

$$\hbar\gamma^{\text{ex}}(T) = c_1 T + \frac{c_2}{e^{\frac{\Omega}{k_B T}} - 1}. \quad (4)$$

All parameters, including c_1 , c_2 , and the average phonon energy Ω , are listed in table II. The parameter φ_0 is the value of the 1s excitonic wave function at the origin in real space [73, 74]. The valley-dependent dipole element \mathbf{d}^{ξ} with $\mathbf{d}^{K^+} \cdot \mathbf{d}^{K^-} = 0$ and absolute value $|\mathbf{d}^{\xi}| = d$ is derived from DFT calculations in Ref. 75.

1. Exciton dipole density as harmonic oscillator

The macroscopic 2d exciton dipole density resulting from the excitonic transition is [76]

$$\mathbf{P}_{\mathbf{q}_{\parallel}}^{\text{ex}} = \sum_{\xi} \varphi_0 \mathbf{d}^{\xi} p_{\mathbf{q}_{\parallel}}^{\xi} + h.c. \quad (5)$$

To achieve an oscillator representation often used in phenomenological models of hybrid MNP-TMDC structures, we apply the Heisenberg equation formalism twice to Eq. (5), similar to Ref. 77 and assume that the damping is small compared to the resonance frequency $(\gamma^{\text{ex}})^2 \ll \omega_{\text{exo}}^2$. For a real-valued electric field $\mathbf{E}_{\mathbf{q}_{\parallel}}(t)$ in the time domain, we find the

following second-order harmonic oscillator for the in-plane components of the dipole density $\mathbf{P}_{\mathbf{q}_{\parallel}}^{\text{ex}}$:

$$(\omega^2 + i\gamma^{\text{ex}}(T)\omega - \omega_{\text{ex}}^2(q_{\parallel})) \mathbf{P}_{\mathbf{q}_{\parallel}}^{\text{ex}} = -\frac{2\omega_{\text{ex}}(q_{\parallel})}{\hbar} |\varphi_0 d|^2 \mathbf{E}_{\mathbf{q}_{\parallel}}(\omega). \quad (6)$$

The z component of \mathbf{P}^{ex} is negligible [78, 79] compared to the in-plane dipole density due to the small thickness of the TMDC.

2. Momentum-Bright Excitons

The dispersion $\omega_{\text{ex}}(\mathbf{q}_{\parallel})$ describes a variety of exciton states with quantum number \mathbf{q}_{\parallel} . Whether an exciton state with $\omega_{\text{ex}}(\mathbf{q}_{\parallel})$ is referred to as bright (○) or dark (●) is characterized by its accessibility under far-field illumination. The corresponding selection rules apply to energy, spin [80], or, as relevant in this case, to momentum \mathbf{q}_{\parallel} . The photon momentum reads $q_{\text{photon}} = \sqrt{\epsilon_{\text{out}}}\frac{\omega}{c}$ and, due to in-plane momentum (\mathbf{q}_{\parallel}) conservation for the excitation process, bright excitons can only possess comparably small in-plane momenta q_{\parallel} :

$$q_{\parallel}^2 < \epsilon_{\text{out}} \frac{\omega^2}{c^2}. \quad (7)$$

Eq. (7) refers to momenta within the light cone. Due to their small momenta, bright excitons are spatially delocalized over large areas in real space (comparable with the wavelength of the incoming light) fulfilling Abbe's diffraction limit. To derive a phenomenological model to fit experiments, we qualitatively consider the $q_{\parallel} = 0$ exciton as a representative mode for all excitons within the light cone since $\omega_{\text{ex}}(q_{\parallel} < \epsilon_{\text{out}}\frac{\omega^2}{c^2}) \approx \omega_{\text{exo}}$ is valid for frequencies ω in the visible range:

$$(\omega^2 + i\gamma_{\circ}^{\text{ex}}(T)\omega - \omega_{\text{exo}}^2) \mathbf{P}_{\mathbf{q}_{\parallel}=0}^{\text{exo}} = -\frac{2\omega_{\text{exo}}}{\hbar} |\varphi_0 d|^2 \mathbf{E}_{\mathbf{q}_{\parallel}=0}, \quad (8)$$

depending on the electric field, Eq. (1). However, we already accounted for the self-interaction \mathbf{E}^{ex} , which gives rise to radiative damping [73], second term in Eq. (9):

$$\gamma_{\circ}^{\text{ex}}(T) = \gamma^{\text{ex}}(T) + |\varphi_0 d|^2 \frac{\omega_{\text{ex}}}{\hbar c \sqrt{\epsilon_{\text{out}} \epsilon_0}}. \quad (9)$$

In Eq. (8) we add the symbol ○ to indicate the brightness of the excitons.

3. Momentum-Dark Excitons

Momentum-dark excitons (●), on the other hand, have larger in-plane momenta,

$$q_{\parallel}^2 > \epsilon_{\text{out}} \frac{\omega^2}{c^2}, \quad (10)$$

positioning them outside the light cone and thus making them optically inaccessible under far-field excitation.

Momentum-dark exciton distributions may have a larger extent in momentum space, enabling them to be spatially localized in real space. The correspondingly generated electric field gradients lead to a momentum-dependent modification of their dispersion:

$$\begin{aligned} & (\omega^2 + i\gamma^{\text{ex}}\omega - \omega_{\text{ex}}^2(q_{\parallel})) \mathbf{P}_{\mathbf{q}_{\parallel}}^{\text{ex}\bullet}(\omega) \\ &= \frac{\omega_{\text{ex}}(q_{\parallel})}{\hbar} |\varphi_0 d|^2 \frac{1}{\varepsilon_0 \varepsilon_{\text{out}}} q_{\parallel} \mathbf{u}_{\phi} \cdot \mathbf{P}_{\mathbf{q}_{\parallel}}^{\text{ex}\bullet} - \frac{2\omega_{\text{ex}}(q_{\parallel})}{\hbar} |\varphi_0 d|^2 \mathbf{E}_{\mathbf{q}_{\parallel}} \end{aligned} \quad (11)$$

where the symbol \bullet indicates the momentum-dark character of the excitons and with the degenerate, idempotent matrix

$$\mathbf{u}_{\phi} = \frac{\mathbf{q}_{\parallel} \otimes \mathbf{q}_{\parallel}}{q_{\parallel}^2} = \begin{pmatrix} \cos^2(\phi) & \cos(\phi)\sin(\phi) \\ \cos(\phi)\sin(\phi) & \sin^2(\phi) \end{pmatrix} \quad (12)$$

depending on the momentum \mathbf{q}_{\parallel} in polar representation (q_{\parallel}, ϕ) , cp. Fig. 3. Similar to the bright excitons, the dark-exciton dynamics are driven by the electric field, Eq. (1), without \mathbf{E}^{ex} as we have singled out the electric field-mediated self-interaction, given by Eq. (12). Despite being optically inaccessible from the far-field, dark excitons may play a crucial role in near-field interactions as we will demonstrate in this manuscript for the context of strong coupling with plasmonic nano-structures.

B. Localized Surface Plasmons

The response of a metal nano-particle with extensions small compared to the incident wavelength, with spheroidal shape and permittivity ε_{MNP} can be described as a point dipole \mathbf{p}^{pl} by Mie-Gans theory [63–65]. In quasi-static approximation, it is given by a polarizability α times the total electric field, cp. Eq. (1), again by excluding the electric field generated by the MNP, i.e., the self interaction.

$$\mathbf{p}^{\text{pl}}(\omega) = \alpha(\omega) \cdot \mathbf{E}(\mathbf{r}_{\text{pl}}, \omega) \quad (13)$$

The polarizability of an oblate metal nano-spheroid is, in a Cartesian basis, diagonal and we choose z to be along the short semi-axis, cp. Fig. 1, such that its entries are $\alpha_x = \alpha_y \neq \alpha_z$ with

$$p_j^{\text{pl}}(\omega) = \alpha_j(\omega) E_j(\mathbf{r}_{\text{pl}}, \omega), \quad (14)$$

and

$$\alpha_j = V_{\text{MNP}} \varepsilon_0 \varepsilon_{\text{out}} \frac{\varepsilon_{\text{MNP}} - \varepsilon_{\text{out}}}{L_j \varepsilon_{\text{MNP}} + (1 - L_j) \varepsilon_{\text{out}}}. \quad (15)$$

V_{MNP} is the volume of the spheroidal MNP

$$V_{\text{MNP}} = \frac{4}{3} \pi r_x^2 r_z \quad (16)$$

and the shape parameters L_j are given by [65]

$$L_z = \frac{1}{e_{\text{MNP}}^2} \left(1 - \frac{\sqrt{1 - e_{\text{MNP}}^2}}{e_{\text{MNP}}} \arcsin(e_{\text{MNP}}) \right) \quad (17)$$

$$\text{and } L_x = L_y = \frac{1 - L_z}{2}, \quad (18)$$

with the spheroids eccentricity

$$e_{\text{MNP}} = 1 - \frac{r_z^2}{r_x^2}. \quad (19)$$

In addition to the geometry, the polarizability α , Eq. (15), depends on the permittivity ε_{out} of the surrounding, cp. Fig. 1, and the permittivity of the MNP itself

$$\varepsilon_{\text{MNP}}(\omega) = \varepsilon_b(\omega) + \chi_d(\omega). \quad (20)$$

The Drude susceptibility, χ_d describes intraband transitions for the quasi-free electrons in the partially occupied metal conduction band. [81, 82]

$$\chi_d(\omega) = \frac{-\omega_{\text{pl,bulk}}^2}{\omega^2 + i\omega\gamma^{\text{pl}}(\omega, T)} \quad (21)$$

with the bulk plasma frequency $\omega_{\text{pl,bulk}}$ and the plasmonic damping $\gamma^{\text{pl}}(\omega, T)$. All other contributions to the MNP susceptibility ε_{MNP} are summarized in the MNP background permittivity

$$\varepsilon_b(\omega) = \varepsilon_{\infty} + \chi_{\text{inter}}(\omega). \quad (22)$$

These include the high-frequency limit dielectric constant ε_{∞} stemming from inner bands and, depending on the chosen metal, frequency dependent inter-band transitions between valence and conduction band in $\chi_{\text{inter}}(\omega)$. In gold, these transitions become significant above 2.4 eV/ \hbar [83]. Although the precise location of visible interband transitions within the gold band structure remains a subject of debate, several models [84–87] have been developed that align well with experimental observations provided in refs. 88 and 89. For this work, we adopt the interband susceptibility described in Ref. 85, given by a sum of Lorentzian functions

$$\chi_{\text{inter}}(\omega) = \sum_{j=1,2} A_j \omega_j \left[\frac{e^{i\phi_j}}{\omega_j - \omega - i\Gamma_j} + \frac{e^{-i\phi_j}}{\omega_i + \omega + i\Gamma_j} \right] \quad (23)$$

In the Drude contribution, Eq. (21), we use a damping rate $\gamma^{\text{pl}}(\omega, T)$ that depends on both temperature and frequency [90–93]. It accounts for electron-electron and electron-phonon scattering:

$$\gamma^{\text{pl}}(\omega, T) = \gamma_{\text{el-el}}^{\text{pl}}(\omega, T) + \gamma_{\text{el-ph}}^{\text{pl}}(T), \quad (24)$$

with [90–93]

$$\gamma_{\text{el-el}}^{\text{pl}}(\omega, T) = \frac{b}{\hbar} [(k_B T)^2 + (\hbar\omega/2\pi)^2], \quad (25)$$

$$\gamma_{\text{el-ph}}^{\text{pl}}(T) = \frac{\gamma_0}{\hbar} \left[\frac{2}{5} + 4 \left(\frac{T}{\Theta} \right)^5 \int_0^{\Theta/T} \frac{z^4}{e^z - 1} dz \right]. \quad (26)$$

Similar to the description of the exciton oscillator, Eqs. (8,11), we combine Eqs. (14)-(21) to obtain an equation for each entry of the plasmon dipole. We assume $\omega E_j(\mathbf{r}_{\text{pl}}) \approx$

0 to be consistent with Eq. (14) that is defined in the quasi-static limit.

$$\begin{aligned} & \left(\omega^2 + i\gamma^{\text{pl}}(\omega, T)\omega - \frac{\omega_{\text{pl,bulk}}^2 L_j}{L_j \varepsilon_b(\omega) + (1 - L_j) \varepsilon_{\text{out}}} \right) p_j^{\text{pl}}(\omega) \\ &= -\frac{\omega_{\text{pl,bulk}}^2 \varepsilon_0 \varepsilon_{\text{out}} V_{\text{MNP}}}{L_j \varepsilon_b(\omega) + (1 - L_j) \varepsilon_{\text{out}}} E_j(\mathbf{r}_{\text{pl}}, \omega) \end{aligned} \quad (27)$$

To obtain a pure classical harmonic oscillator model from Eq. (27), we approximate $\varepsilon_b(\omega) \approx \text{Re} \varepsilon_b(\omega_{\text{lsp}}) \equiv \varepsilon_b$, $\gamma^{\text{pl}}(\omega, T) \approx \gamma^{\text{pl}}(\omega_{\text{lsp}}, T) \equiv \gamma^{\text{pl}}(T)$ by dropping the respective frequency dependencies in the relevant frequency range with $E_j(\omega; \mathbf{r}_{\text{pl}}) \neq 0$ which we therefore restrict to the frequency regime where $\hbar\omega < 2.4 \text{ eV}$ [83]. This approximation is necessary to treat the plasmon dipole as a single harmonic oscillator, and it resembles the main weakness of this simplified model for the MNP dynamics. Thus, the inner metal shells and interband transition contributions to the permittivity are treated parametrically in the macroscopic Maxwell equations, therefore altering the electric field solution. Implications of this approximation are discussed in Appendix D. In the case of the spheroid, the geometry breaks the symmetry between the in-plane (x/y) and z -direction. However, the coupling to the TMDC excitons is dominated by the x/y -components of the MNP dipole that is chosen to be resonant or near-resonant to the TMDC excitons and orientated parallel to the TMDC plane [15], cp. Fig. 1. We provide a detailed justification for dropping the z -direction in Sec. III and Appendix B. All in all, Eq. (27) simplifies to a single harmonic oscillator equation for the relevant (in-plane) plasmon dipole contribution \mathbf{p}^{pl} :

$$(\omega^2 + i\gamma^{\text{pl}}(T)\omega - \omega_{\text{lsp}}^2) \mathbf{p}^{\text{pl}}(\omega) = -V_{\text{MNP}} \frac{\varepsilon_0 \varepsilon_{\text{out}}}{L} \omega_{\text{lsp}}^2 \mathbf{E}(\omega; \mathbf{r}_{\text{pl}}) \quad (28)$$

with the localized surface plasmon (LSP) frequency of the MNP,

$$\omega_{\text{lsp}} = \sqrt{\frac{\omega_{\text{pl,bulk}}^2 L}{L \varepsilon_b + (1 - L) \varepsilon_{\text{out}}}}, \quad (29)$$

which differs from the bulk plasma frequency $\omega_{\text{pl,bulk}}$ due to the influence of the MNP geometry via the shape factor L , Eq. (18), and the background ε_b as well as the surrounding permittivity ε_{out} .

III. EXCITON-PLASMON COUPLING

Now we turn to the description of the exciton-plasmon coupling. Exciton and plasmon interact via the total electric field, cp. Eq. (1), such that the previously derived individual harmonic oscillator Eqs. (8,11,28) couple. When inserting the occurring electric fields, we have to consider, that the self-interaction generated by the MNP and TMDC respectively has already been self-consistently taken into account in their individual harmonic oscillator dynamics. Considering the cross-field interaction via \mathbf{E}^{ex} and \mathbf{E}^{pl} and the incident field \mathbf{E}^0 ,

we obtain a set of coupled harmonic oscillator equations - the bright exciton oscillator equation

$$\begin{aligned} & (\omega^2 + i\gamma_{\text{o}}^{\text{ex}}\omega - \omega_{\text{exo}}^2) \mathbf{P}_{\mathbf{q}_{\parallel}=\mathbf{0}}^{\text{exo}}(\omega) \\ &= -\frac{2\omega_{\text{exo}}}{\hbar} |\varphi_0 d|^2 \left(\mathbf{E}_{\mathbf{q}_{\parallel}=\mathbf{0}}^{\text{pl}}(z_{\text{ex}}; \omega) + \mathbf{E}_{\mathbf{q}_{\parallel}=\mathbf{0}}^0(z_{\text{ex}}; \omega) \right), \end{aligned} \quad (30)$$

one oscillator equation for each momentum-dark exciton, with momenta $q_{\parallel} > \sqrt{\varepsilon_{\text{out}}} \frac{\omega}{c}$,

$$\begin{aligned} & \left((\omega^2 + i\gamma^{\text{ex}}\omega - \omega_{\text{ex}}^2(q_{\parallel})) \mathbb{1} - \frac{\omega_{\text{ex}}(q_{\parallel})}{\hbar} \frac{|\varphi_0 d|^2}{\varepsilon_0 \varepsilon_{\text{out}}} q_{\parallel} \mathcal{U}_{\phi} \right) \cdot \mathbf{P}_{\mathbf{q}_{\parallel}}^{\text{ex}\bullet}(\omega) \\ &= -\frac{2\omega_{\text{ex}}(q_{\parallel})}{\hbar} |\varphi_0 d|^2 \left(\mathbf{E}_{\mathbf{q}_{\parallel}}^{\text{pl}}(z_{\text{ex}}; \omega) + \mathbf{E}_{\mathbf{q}_{\parallel}}^0(z_{\text{ex}}; \omega) \right), \end{aligned} \quad (31)$$

and the plasmon oscillator equation

$$\begin{aligned} & (\omega^2 + i\gamma^{\text{pl}}\omega - \omega_{\text{lsp}}^2) \mathbf{p}^{\text{pl}}(\omega) \\ &= -V_{\text{MNP}} \frac{\varepsilon_0 \varepsilon_{\text{out}}}{L} \omega_{\text{lsp}}^2 \left(\mathbf{E}^{\text{ex}}(\mathbf{r}_{\text{pl}}; \omega) + \mathbf{E}^0(\mathbf{r}_{\text{pl}}; \omega) \right). \end{aligned} \quad (32)$$

The electric field emitted by the TMDC excitons at an arbitrary position z is expressed via the dyadic Green's function \mathcal{G} and transformed to real space, similar to Ref. 13. Without loss of generality, we set the in-plane coordinate of the MNP to $\mathbf{r}_{\parallel \text{MNP}} = \mathbf{0}$. Expressing the fields by their sources, we have:

$$\mathbf{E}^{\text{exo}/\bullet}(\mathbf{r}_{\text{pl}}; \omega) = \frac{1}{(2\pi)^2} \int d^2 q_{\parallel} \mathcal{G}_{\mathbf{q}_{\parallel}}(z_{\text{pl}}, z_{\text{ex}}; \omega) \cdot \mathbf{P}_{\mathbf{q}_{\parallel}}^{\text{exo}/\bullet}(\omega). \quad (33)$$

Analogous, the electric field emitted by the MNP in momentum space and observed in the TMDC layer at z_{ex} is given by

$$\mathbf{E}_{\mathbf{q}_{\parallel}}^{\text{pl}}(z_{\text{ex}}; \omega) = \mathcal{G}_{\mathbf{q}_{\parallel}}(z_{\text{ex}}, z_{\text{pl}}; \omega) \cdot \mathbf{p}^{\text{pl}}(\omega). \quad (34)$$

For an incident field $\mathbf{E}_{\mathbf{q}_{\parallel}, \mathbf{0}}^0$ with only in-plane electric field components, such as a plane wave propagating perpendicular to the TMDC, neither the TMDC nor the MNP polarization gain a contribution in z -direction. Therefore, we may drop all z -components in the following, which reduces the effective dimension of Eqs. (30-32) each to two. We provide a formal proof that this effective 2d theory in fact resembles the coupling in the 3d hybrid structure in Appendix B. Thus, without approximation, the dyadic Green's function reduces to 2×2 with

$$\mathcal{G}_{\mathbf{q}_{\parallel}}(z, z', \omega) = \left(-\frac{\omega^2}{\varepsilon_0 c^2} \mathbb{1} + \frac{\mathbf{q}_{\parallel} \otimes \mathbf{q}_{\parallel}}{\varepsilon_0 \varepsilon_{\text{out}}} \right) G_{q_{\parallel}}(z, z', \omega). \quad (35)$$

For simplicity, we apply the scalar Green's function for a homogeneous dielectric environment

$$G_{q_{\parallel}}(z, z', \omega) = \frac{-i}{2k_{q_{\parallel}}} e^{ik_{q_{\parallel}}|z-z'|} \quad (36)$$

with the wavevector $k_{q_{\parallel}} = \sqrt{\frac{\varepsilon_{\text{out}}}{c^2} \omega^2 - q_{\parallel}^2}$.

Combining Eqs. (32, 34 and 35) shows that the MNP provides high \mathbf{q}_{\parallel} (evanescent) electric fields, that allow to access originally momentum-dark excitons in the TMDC,

cp. Eq. (31). Furthermore, from Eqs. (13-15) it follows that, for a plane-wave excitation propagating along z , the orientation of the MNP dipole \mathbf{p}^{pl} directly follows the orientation of the electric field $\mathbf{E}(\mathbf{r}_{\text{pl}})$. Consequently, a circular (σ) polarized incident electric field \mathbf{E}^0 yields $\mathbf{p}^{\text{pl}} \parallel \mathbf{e}_\sigma$. However, a circularly polarized oriented point dipole does not generate a uniformly circular polarized electric near-field, cp. Eqs. (34,35). In contrast, its electric near-field possesses contributions in both circular polarization directions, depending on the relative position to the MNP. Consequently, even for circularly polarized excitation, the MNP acts as an excitation and couples to excitons in both valleys K^+ and K^- . [94] In the next three sections (III A, III B and III C) we simplify the action of the interacting fields in the coupled equations (30,31,32) to obtain a simplified system of three coupled oscillators, which can be used to fit experiments.

A. Coupled oscillator equation for momentum-dark excitons

Due to the vicinity of plasmon and excitons within a small fraction of the wavelength, we apply the quasi-static approximation [95] to describe their mutual near-field interactions. This limit for the dyadic Green's function, occurring in Eqs. (33,34), corresponds to neglecting the frequency compared to the near-field momentum:

$$\varepsilon_{\text{out}} \frac{\omega^2}{c^2} \ll q_{\parallel}^2. \quad (37)$$

This assumption is valid for exciton dipole density contributions with high momenta \mathbf{q}_{\parallel} , i.e., outside the light-cone, Eq. (10). In contrast, the momentum-bright excitons ($q_{\parallel} = 0$) excited by the incident electric field $\mathbf{E}_{\mathbf{q}_{\parallel}=0}^0$ within the light-cone are described with the full frequency dependency separately in Sec. III C. For momentum-dark excitons, the dyadic Green's function in quasi-static approximation simplifies to

$$\mathcal{G}_{\mathbf{q}_{\parallel}}(z, z') = G_{\mathbf{q}_{\parallel}}(z, z') \frac{q_{\parallel}^2}{\varepsilon_0 \varepsilon_{\text{out}}} \mathbf{u}_\phi \quad (38)$$

with (q_{\parallel}, ϕ) the polar coordinates of \mathbf{q}_{\parallel} , as illustrated in Fig. 3 and the degenerate, idempotent matrix \mathbf{u}_ϕ , Eq. (12). Using the quasi-static scalar Green's functions

$$G_{\mathbf{q}_{\parallel}}(z, z') = \frac{-1}{2q_{\parallel}} e^{-q_{\parallel}|z-z'|}, \quad (39)$$

we obtain

$$\mathcal{G}_{\mathbf{q}_{\parallel}}(z_{\text{pl}}, z_{\text{ex}}) = \frac{-1}{2\varepsilon_0 \varepsilon_{\text{out}}} q_{\parallel} e^{-q_{\parallel} \delta z} \mathbf{u}_\phi, \quad (40)$$

where $\delta z = |z_{\text{ex}} - z_{\text{Au}}|$ denotes the center to center distance of TMDC and MNP, cp. Fig. 1. Consequently, the plasmon electric field experienced by the excitons, Eq. (34), becomes

$$\mathbf{E}_{\mathbf{q}_{\parallel}}^{\text{pl}}(z_{\text{ex}}; \omega) = \frac{-1}{2\varepsilon_0 \varepsilon_{\text{out}}} q_{\parallel} e^{-q_{\parallel} \delta z} \mathbf{u}_\phi \cdot \mathbf{p}^{\text{pl}}(\omega). \quad (41)$$

We first insert the plasmons electric field, Eq. (41), in the oscillator equation for momentum-dark excitons, Eq. (31),

$$\begin{aligned} & (\omega^2 + i\gamma^{\text{ex}}\omega - \omega_{\text{ex}}^2(q_{\parallel})) \mathbf{P}_{\mathbf{q}_{\parallel}}^{\text{ex}\bullet} \\ &= \frac{\omega_{\text{ex}}(q_{\parallel})}{\hbar} \frac{|\varphi_0 d|^2}{\varepsilon_0 \varepsilon_{\text{out}}} q_{\parallel} \mathbf{u}_\phi \cdot \left(\mathbf{P}_{\mathbf{q}_{\parallel}}^{\text{ex}\bullet}(\omega) + e^{-q_{\parallel} \delta z} \mathbf{p}^{\text{pl}}(\omega) \right). \end{aligned} \quad (42)$$

Since our goal is to provide an analytic approach to fit experiments, we apply here a separation ansatz for time and polar momentum dependencies of the excitonic polarization

$$\mathbf{P}_{\mathbf{q}_{\parallel}}^{\text{ex}\bullet}(\omega) = P_{q_{\parallel}}^{\text{ex}\bullet} \mathbf{u}_\phi \cdot \mathbf{P}^{\text{ex}\bullet}(\omega) \quad (43)$$

Inserting this separation ansatz into Eq. (42), and integrating over the polar angle ϕ yields

$$\begin{aligned} & (\omega^2 + i\gamma^{\text{ex}}\omega - \omega_{\text{ex}\bullet}^2(q_{\parallel})) P_{q_{\parallel}}^{\text{ex}\bullet} \mathbf{P}^{\text{ex}\bullet}(\omega) \\ &= \frac{\omega_{\text{ex}}(q_{\parallel})}{\hbar} \frac{|\varphi_0 d|^2}{\varepsilon_0 \varepsilon_{\text{out}}} q_{\parallel} e^{-q_{\parallel} \delta z} \mathbf{p}^{\text{pl}}(\omega), \end{aligned} \quad (44)$$

where the momentum-dark exciton resonance $\omega_{\text{ex}\bullet}(q_{\parallel})$ appears at:

$$\omega_{\text{ex}\bullet}^2(q_{\parallel}) = \omega_{\text{ex}}^2(q_{\parallel}) + \frac{\omega_{\text{ex}}(q_{\parallel})}{\hbar} \frac{|\varphi_0 d|^2}{\varepsilon_0 \varepsilon_{\text{out}}} q_{\parallel}. \quad (45)$$

Similar to refs. 96 and 97, the modification to the free exciton $\omega_{\text{ex}}(q_{\parallel})$, stemming from the electric field mediated exciton self-interaction, can be considered a polaritonic correction. The modified exciton-polariton dispersion, Eq. (45), is displayed in Fig. 3. With Eq. (44) we thus encounter a distinct harmonic oscillator equation for the momentum-dark excitons with different momenta corresponding to different energies. In order to simplify Eq. (44) for all q_{\parallel} to a single equation, all these $q_{\parallel} \neq 0$ excitons are collected into a single, effective exciton mode. This is accomplished by introducing the exciton resonance frequency $\omega_{\text{ex}\bullet}^2(q_{\parallel})$ at a single effective momentum q_{eff} . We define $\omega_{\text{ex}\bullet}^2(q_{\parallel}) \approx \omega_{\text{ex}\bullet}^2(q_{\text{eff}}) \equiv \omega_{\text{ex}\bullet}^2$ (horizontal dotted line in Fig. 3). This approximation is crucial to recover the important physics beyond a fully phenomenological oscillator model, by introducing a collective dark exciton state. For simplicity, we furthermore assume for the free exciton dispersion, Eq. (3), $\omega_{\text{ex}}(q_{\parallel}) \approx \omega_{\text{ex}0}$, where we neglect the quadratic contribution that is small compared to both, $\omega_{\text{ex}0}$ and the linear q_{eff} dependent correction. This allows to solve the momentum dependency of Eq. (44) with the distribution

$$P_{q_{\parallel}}^{\text{ex}\bullet} = q_{\parallel} \delta z e^{-q_{\parallel} \delta z}, \quad (46)$$

which we depict in Fig. 3 with parameters provided in table II. Obviously, the momentum-dark exciton, Eq. (46), vanishes at $q_{\parallel} = 0$. [72] We determine the effective exciton momentum q_{eff} (vertical dotted lines in Fig. 3) as the averaged absolute value of the momentum regarding the 2D-momentum distribution, Eq. (46):

$$q_{\text{eff}} = \frac{\int_{\mathbb{R}^2} d^2 \mathbf{q}_{\parallel} q_{\parallel} P_{q_{\parallel}}^{\text{ex}\bullet}}{\int_{\mathbb{R}^2} d^2 \mathbf{q}_{\parallel} P_{q_{\parallel}}^{\text{ex}\bullet}} = \frac{3}{\delta z} \quad (47)$$

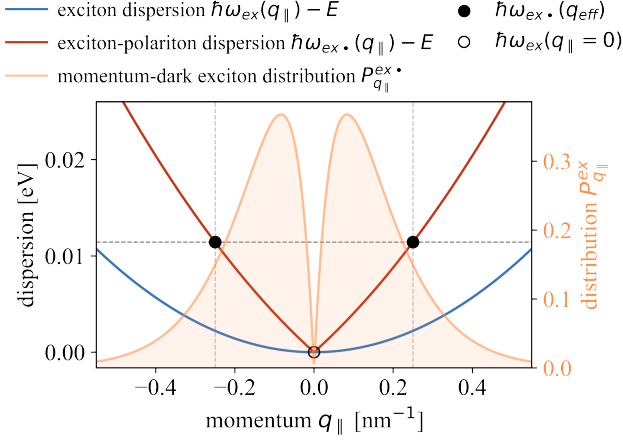


Figure 3. Dispersion relations for exciton respectively exciton-polariton states. The solid lines represent the original exciton ($\hbar\omega_{ex}$) and modified exciton-polariton ($\hbar\omega_{ex\bullet}$) energies as functions of the momentum $q_{||}$. The orange curve shows the exciton distribution $P_{q_{||}}^{ex\bullet}$ with regard to its ordinate axis on the right side. Vertical dashed lines indicate the effective exciton momentum q_{eff} . The horizontal dashed line marks the energy $\hbar\omega_{ex\bullet}(q_{eff})$ of the effective exciton mode.

For the frequency dependency of the momentum-dark excitons, we find

$$(\omega^2 + i\gamma^{ex}\omega - \omega_{ex\bullet}^2) \mathbf{P}^{ex\bullet}(\omega) = \frac{\omega_{ex\bullet}}{\hbar\delta z} \frac{|\varphi_0 d|^2}{\varepsilon_0 \varepsilon_{out}} \mathbf{P}^{pl}(\omega). \quad (48)$$

In the time domain, Eq. (48) corresponds to a harmonic oscillator for the collective momentum-dark exciton mode coupled to the plasmon:

$$(\partial_t^2 + \gamma^{ex}\partial_t + \omega_{ex\bullet}^2) \mathbf{P}^{ex\bullet}(t) + \frac{\omega_{ex\bullet}}{\hbar\delta z} \frac{|\varphi_0 d|^2}{\varepsilon_0 \varepsilon_{out}} \mathbf{P}^{pl}(t) = 0 \quad (49)$$

The convention of the applied Fourier transform are specified in Appendix A.

B. Coupled oscillator equation for the MNP plasmon

The solution for the dark exciton momentum dependency allows to simplify the expression for their coupling to the plasmon. From $\frac{q_{eff}^2}{\varepsilon_{out}} \gg \frac{\omega^2}{c^2}$ in the Green's dyadic, Eq. (35), for MNPs significantly smaller than the wavelength of the incident light, it follows that the action of bright excitons ($q_{||} \approx 0$) to the MNP plasmon dynamics can be neglected in Eq. (33), compared to the near-field stemming from momentum-dark excitons. The electric field, Eq. (33), of the momentum-dark excitons can be treated in quasi-static approximation, similar to the previous section. It simplifies to

$$\mathbf{E}^{ex}(\mathbf{r}_{pl}; \omega) = \frac{-1}{2\varepsilon_0 \varepsilon_{out}} \frac{1}{(2\pi)^2} \int d^2 q_{||} q_{||} e^{-q_{||} \delta z} \mathcal{U}_\phi \cdot \mathbf{P}_{q_{||}}^{ex\bullet}(\omega). \quad (50)$$

Inserting the exciton momentum distribution, Eqs. (43,46), in its emitted electric near-field, Eq. (50), yields

$$\mathbf{E}^{ex}(\mathbf{r}_{pl}; \omega) = \frac{-1}{4\pi\varepsilon_0 \varepsilon_{out}} \frac{3}{16} \frac{1}{(\delta z)^3} \mathbf{P}^{ex\bullet}(\omega). \quad (51)$$

Thus, from Eqs. (32,51), we find for the plasmon

$$\begin{aligned} (\omega^2 + i\gamma^{pl}(T)\omega - \omega_{lsp}^2) \mathbf{P}^{pl}(\omega) - \omega_{lsp}^2 \frac{V_{MNP}}{L} \frac{3}{64\pi} \frac{1}{\delta z^3} \mathbf{P}^{ex\bullet}(\omega) \\ = -\omega_{lsp}^2 \frac{V_{MNP}}{L} \varepsilon_0 \varepsilon_{out} \mathbf{E}^0(\mathbf{r}_{pl}; \omega). \end{aligned} \quad (52)$$

In the time domain, Eq. (52) yields a harmonic oscillator equation for the MNP plasmon \mathbf{P}^{pl} coupled to the collective momentum-dark exciton mode $\mathbf{P}^{ex\bullet}$:

$$\begin{aligned} (\partial_t^2 + \gamma^{pl}(T)\partial_t + \omega_{lsp}^2) \mathbf{P}^{pl}(t) + \omega_{lsp}^2 \frac{V_{MNP}}{L} \frac{3}{64\pi} \frac{1}{\delta z^3} \mathbf{P}^{ex\bullet}(t) \\ = \omega_{lsp}^2 \frac{V_{MNP}}{L} \varepsilon_0 \varepsilon_{out} \mathbf{E}^0(\mathbf{r}_{pl}; t). \end{aligned} \quad (53)$$

C. Coupled oscillator equation for bright excitons

In the previous section, we restricted ourselves to the near-field where excitons with high momenta, Eq. (10), and plasmons interact with evanescent electric fields. However, excitons with small momenta, cp. Eq. (7), may also contribute to the optical spectra. In fact, they dominate it for a pristine TMDC since excitons outside the light cone are not excited by far field excitation without the presence of the MNP (or another source that breaks translational invariance and thus provides an evanescent electric field). To incorporate the bright excitons in the coupled model, we explicitly insert the electric field generated by the MNP, Eq. (34), evaluated at $\mathbf{q}_{||} = 0$,

$$\mathbf{E}_{\mathbf{q}_{||}=0}^{pl}(z_{ex}, \omega) = i\omega \frac{1}{2c} \frac{1}{\varepsilon_0 \sqrt{\varepsilon_{out}}} \mathbf{P}^{pl}(\omega) e^{i\frac{\sqrt{\varepsilon_{out}}}{c} \delta z \omega}, \quad (54)$$

in the bright exciton dynamics, Eq. (30). Transforming into time domain, the frequency prefactor becomes a time derivative and the exponential yields a time delay. We obtain

$$\begin{aligned} (\partial_t^2 + \gamma_{\circ}^{ex}\partial_t + \omega_{ex\bullet}^2) \mathbf{P}_{\mathbf{q}_{||}=0}^{ex\bullet}(t) \\ = \frac{2\omega_{ex}}{\hbar} |\varphi_0 d|^2 \left[\mathbf{E}_{\mathbf{q}_{||}=0}^0(z_{ex}; t) - \frac{1}{2c\sqrt{\varepsilon_{out}}\varepsilon_0} \partial_t \mathbf{P}^{pl}(t - \delta t) \right], \end{aligned} \quad (55)$$

where $\delta t = \frac{\sqrt{\varepsilon_{out}}}{c} \delta z$ is the propagation time of light from the plasmon position to the TMDC plane.

D. Three Coupled Oscillators Model (3-COM)

In the previous sections, we found three coupled harmonic oscillators that effectively model the temporal dynamics of the TMDC-MNP hybrid: the plasmon, the collective momentum-dark exciton and the bright exciton oscillator equations. In the

following, we summarize these oscillator contributions to the coupled TMDC-MNP dynamics:

Three Coupled Oscillators Model (3-COM) (56)

$$\begin{aligned} (\partial_t^2 + \gamma^{\text{pl}}(T)\partial_t + \omega_{\text{isp}}^2) \mathbf{P}^{\text{pl}}(t) + g^{\text{pl}}\mathbf{P}^{\text{ex}\bullet}(t) &= f^{\text{pl}}\mathbf{E}^0(\mathbf{r}_{\text{pl}}; t) \\ (\partial_t^2 + \gamma^{\text{ex}}(T)\partial_t + \omega_{\text{ex}\bullet}^2) \mathbf{P}^{\text{ex}\bullet}(t) + g_{\bullet}^{\text{ex}}\mathbf{P}^{\text{pl}}(t) &= 0 \\ (\partial_t^2 + \gamma_{\circ}^{\text{ex}}(T)\partial_t + \omega_{\text{ex}\circ}^2) \mathbf{P}_{\mathbf{q}_{\parallel}=0}^{\text{ex}\circ}(t) + g_{\circ}^{\text{ex}}\partial_t\mathbf{P}^{\text{pl}}(t - \delta t) &= f_{\circ}^{\text{ex}}\mathbf{E}_{\mathbf{q}_{\parallel}=0}^0(z_{\text{ex}}; t) \end{aligned}$$

An overview of the occurring parameters is given in table I. Equation (56) shows that the system is reduced to the coupled dynamics of three oscillators: The incident electric field directly drives the MNP plasmon and the bright exciton. On the other hand, the momentum-dark exciton couples to the MNP plasmon via the coupling strength g_{\bullet}^{ex} , and vice versa via g^{pl} . The temporal gradient of the MNP plasmon, with a time delay δt , corresponding to the light propagation time over the

distance δz , and coupling strength g_{\circ}^{ex} , affects the bright exciton mode. The impact of the momentum bright exciton on the MNP plasmon is negligible. The first two lines in Eq. (56) are similar to the common COM as given in Ref. 32, but we note that here the momentum-dark exciton frequency $\omega_{\text{ex}\bullet}$ differs from the bright exciton frequency $\omega_{\text{ex}\circ}$ as observed in far-field spectroscopy. The inclusion of the third oscillator, the bright exciton with its qualitatively different coupling to the MNP plasmon, represents an extension to the common COM.

To solve the coupled set of harmonic oscillators, we make a plane wave ansatz for the incident electric field propagating along the z -direction

$$\mathbf{E}^0(\mathbf{r}, t) = \mathbf{E}^0 \text{Re} (e^{ikz - i\omega t}) = \mathbf{E}^0 \cos(kz - \omega t) \quad (57)$$

with $k = \sqrt{\varepsilon_{\text{out}}}\frac{\omega}{c}$ and the in-plane polarized amplitude \mathbf{E}^0 . We solve the coupled set of equations via a Fourier transform, which is straight forward for the complex representation of the electric field and dipole densities. As a last step, we take the real part of the coupled set of linear equations. The solution for the temporal plasmon, momentum-dark exciton and bright exciton dynamics is given by:

$$\mathbf{P}^{\text{pl}}(t) = -\text{Re} \left(\frac{(\omega^2 + i\omega\gamma^{\text{ex}} - \omega_{\text{ex}\bullet}^2)}{(\omega^2 + i\omega\gamma^{\text{pl}} - \omega_{\text{isp}}^2)(\omega^2 + i\omega\gamma^{\text{ex}} - \omega_{\text{ex}\bullet}^2) - g^{\text{pl}}g_{\bullet}^{\text{ex}}} e^{ikz_{\text{pl}} - i\omega t} \right) f^{\text{pl}} \mathbf{E}^0 \quad (58)$$

$$\mathbf{P}^{\text{ex}\bullet}(t) = -\text{Re} \left(\frac{g_{\bullet}^{\text{ex}}}{(\omega^2 + i\omega\gamma^{\text{pl}} - \omega_{\text{isp}}^2)(\omega^2 + i\omega\gamma^{\text{ex}} - \omega_{\text{ex}\bullet}^2) - g^{\text{pl}}g_{\bullet}^{\text{ex}}} e^{ikz_{\text{pl}} - i\omega t} \right) f^{\text{pl}} \mathbf{E}^0 \quad (59)$$

$$\mathbf{P}_{\mathbf{q}_{\parallel}=0}^{\text{ex}\circ}(t) = -\text{Re} \left(\frac{1}{\omega^2 + i\gamma_{\circ}^{\text{ex}}\omega - \omega_{\text{ex}\circ}^2} e^{ikz_{\text{ex}} - i\omega t} \right) (2\pi)^2 \delta(\mathbf{q}_{\parallel}) f_{\circ}^{\text{ex}} \mathbf{E}^0 \quad (60)$$

For the bright exciton, we neglect the coupling to the plasmon that is weak since $g^{\text{pl}}, g_{\bullet}^{\text{ex}} \gg g_{\circ}^{\text{ex}}$. If taken into account, it acts as an additional contribution to the damping $\gamma^{\text{ex}\circ}$ of the bright exciton [66]. Considering the definitions in table I, we find for a symmetrized form of the coupled oscillators, Eq. (56), the effective coupling strength between momentum-dark exciton and plasmon

$$g_{\text{eff}} = \sqrt{g^{\text{pl}}g_{\bullet}^{\text{ex}}} \sim \begin{cases} \sqrt{V_{\text{MNP}}} \\ \delta z^{-2} \end{cases} \quad (61)$$

that depends on the MNP volume V_{MNP} and the exciton-plasmon distance δz . Due to the 2d-geometry, the derived distance dependency differs from the coupling of a MNP plasmon to a 0d exciton [42, 98, 99], which typically follows δz^{-3} . It is important to note that the dependence of g_{eff} on the surrounding permittivity ε_{out} , as discussed in Ref. 100, cannot be accurately captured within such a simplified oscillator model. For further details, see Appendix D.

The bright ($q_{\parallel} = 0$) exciton mode shows no spatial depen-

dence

$$\mathbf{P}^{\text{ex}\circ}(\mathbf{r}; t) = -\text{Re} \left(\frac{1}{\omega^2 + i\gamma_{\circ}^{\text{ex}}\omega - \omega_{\text{ex}\circ}^2} e^{ikz_{\text{ex}} - i\omega t} \right) f_{\circ}^{\text{ex}} \mathbf{E}^0, \quad (62)$$

and exists independently on the localized exciton distribution [94] stemming from momentum-dark excitons.

E. Observables

Corresponding to energy balance, the absorbed energy W_{abs} is given by the extinction W_{ext} and the radiated energy W_{rad} :

$$W_{\text{abs}} = W_{\text{ext}} + W_{\text{rad}}, \quad (63)$$

where $W_{\text{rad}} < 0$ since it is out-going energy, re-radiated respectively scattered by the system, cp. Fig. 1. The energy absorbed within the volume V and observation time τ is given

Table I. Parameter definitions for the 3-COM

MNP plasmon	\mathbf{p}^{pl}
momentum-dark exciton	$\mathbf{P}^{\text{ex}\bullet}$
bright exciton	\mathbf{P}^{exo}
incident electric field	\mathbf{E}^0
localized surface plasmon frequency	$\omega_{\text{lsp}} = \omega_{\text{pl,bulk}} \sqrt{\frac{L}{L\epsilon_b + (1-L)\epsilon_{\text{out}}}}$
dark exciton frequency	$\omega_{\text{ex}\bullet} = \sqrt{\omega_{\text{ex}\bullet}^2 + \frac{\omega_{\text{ex}\bullet} \varphi_0 d ^2 q_{\text{eff}}}{\hbar \epsilon_0 \epsilon_{\text{out}}}}$
eff. dark exciton momentum	$q_{\text{eff}} = \frac{3}{\delta z}$
bright exciton frequency	ω_{exo}
plasmon coupling constant	$g^{\text{pl}} = \omega_{\text{lsp}}^2 \frac{V_{\text{MNP}}}{L} \frac{3}{64\pi} \frac{1}{\delta z^3}$
dark exciton coupling constant	$g_{\bullet}^{\text{ex}} = \frac{\omega_{\text{ex}\bullet}}{\hbar} \varphi_0 d ^2 \frac{1}{\epsilon_0 \epsilon_{\text{out}}} \frac{1}{\delta z}$
effective coupling constant	$g_{\text{eff}} = \sqrt{g^{\text{pl}} g_{\bullet}^{\text{ex}}}$
bright exciton coupling constant	$g_{\circ}^{\text{ex}} = \frac{\omega_{\text{exo}}}{\hbar} \varphi_0 d ^2 \frac{1}{\sqrt{\epsilon_{\text{out}} \epsilon_0}} \frac{1}{c}$
propagation time of light	$\delta t = \frac{\sqrt{\epsilon_{\text{out}}}}{c} \delta z$
plasmon oscillator strength	$f^{\text{pl}} = \omega_{\text{lsp}}^2 \frac{V_{\text{MNP}}}{L} \epsilon_0 \epsilon_{\text{out}}$
bright exciton oscillator strength	$f_{\circ}^{\text{ex}} = \frac{2\omega_{\text{exo}}}{\hbar} \varphi_0 d ^2$
plasmon damping constant	$\gamma^{\text{pl}}(T)$, see Eqs. (24-26)
dark exciton damping constant	$\gamma^{\text{ex}}(T)$, see Eq. (4)
bright exciton damping constant	$\gamma_{\circ}^{\text{ex}}(T)$, see Eqs. (4,9)

by [95]

$$W_{\text{abs}} = \int_{\tau} dt \int_V d^3 r \mathbf{E}(\mathbf{r}, t) \cdot \dot{\mathbf{P}}(\mathbf{r}, t). \quad (64)$$

A detailed analysis of all arising terms is given in Appendix C. In the following, we focus on the contributions to connect the derived solution for the coupled plasmon-exciton dynamics with measurable optical properties. We provide results for the extinction (Sec. III E 1), experimentally accessible via linear transmission and reflection [46, 48–52, 54, 60, 101, 102], and

scattering cross section (Sec. III E 2) as measured in dark-field spectroscopy [6, 21, 47, 55–59, 103].

I. Extinction

The extinction is the energy absorbed and scattered by the system that equals the work done by the incident electric field at the MNP plasmon and the TMDC exciton, cp. Appendix C.

$$W_{\text{ext}} = \int_{\tau} dt \int_V d^3 r \mathbf{E}^0(\mathbf{r}, t) \cdot \dot{\mathbf{P}}(\mathbf{r}, t) \quad (65)$$

Since the incident electric field $\mathbf{E}^0 \delta_{\mathbf{q}_{\parallel}, 0}$ acts directly only on originally bright excitons ($q_{\parallel} = 0$) that have been approximated by a constant 2d dipole density and the MNP plasmon within the laser spot with area A , only the coupling of these terms to the incident field \mathbf{E}^0 contributes. Therefore, we define with respect to the measured far-field extinction

$$W_{\text{ext}} = W_{\text{ext}}^{\text{pl}} + W_{\text{ext}}^{\text{exo}} \quad (66)$$

with the plasmon and bright exciton extinctions

$$W_{\text{ext}}^{\text{pl}} = \int_{\tau} dt \mathbf{E}^0(\mathbf{r}_{\text{pl}}, t) \cdot \dot{\mathbf{p}}^{\text{pl}}(t), \quad (67)$$

$$W_{\text{ext}}^{\text{exo}} = A \int_{\tau} dt \mathbf{E}^0(\mathbf{r}_{\parallel}, z_{\text{ex}}, t) \cdot \dot{\mathbf{P}}^{\text{exo}}(\mathbf{r}_{\parallel}, t). \quad (68)$$

Since the observation time τ is significantly longer than a period of the incident light $\tau \gg \frac{2\pi}{\omega}$, we average over the carrier frequency oscillation. To determine the normalized extinction w_{ext} , we divide the work done at the hybrid structure W_{ext} by the in-coming energy

$$W^0 = A\tau \frac{\sqrt{\epsilon_{\text{out}}}}{2} \epsilon_0 c |\mathbf{E}^0|^2 \quad (69)$$

on the illuminated area A during time τ . We obtain the normalized plasmon-exciton extinction

$$w_{\text{ext}} = \frac{W_{\text{ext}}^{\text{pl}} + W_{\text{ext}}^{\text{exo}}}{W^0} = w_{\text{ext}}^{\text{pl}} + w_{\text{ext}}^{\text{exo}}. \quad (70)$$

Inserting the solved exciton and plasmon dynamics from the previous section, Eqs. (58,59,62), and the incident electric field, Eq. (57), we obtain:

$$\text{Normalized Extinction } w_{\text{ext}} = w_{\text{ext}}^{\text{pl}} + w_{\text{ext}}^{\text{exo}} \quad (71)$$

$$w_{\text{ext}}^{\text{pl}} = -\frac{1}{A} \frac{\omega f^{\text{pl}}}{c \epsilon_0 \sqrt{\epsilon_{\text{out}}}} \text{Im} \left(\frac{(\omega^2 + i\gamma^{\text{ex}}\omega - \omega_{\text{ex}\bullet}^2)}{(\omega^2 + i\gamma^{\text{ex}}\omega - \omega_{\text{ex}\bullet}^2)(\omega^2 + i\gamma^{\text{pl}}\omega - \omega_{\text{lsp}}^2) - g^{\text{pl}} g_{\bullet}^{\text{ex}}} \right)$$

$$w_{\text{ext}}^{\text{exo}} = -\frac{\omega f_{\circ}^{\text{ex}}}{c \epsilon_0 \sqrt{\epsilon_{\text{out}}}} \text{Im} \left(\frac{1}{\omega^2 + i\gamma_{\circ}^{\text{ex}}\omega - \omega_{\text{exo}}^2} \right)$$

The MNP plasmon contribution $w_{\text{ext}}^{\text{pl}}$ is qualitatively similar to the commonly applied COM [32]. However, we obtain additionally the bright exciton contribution $w_{\text{ext}}^{\text{ex}}$ for TMDC exciton-MNP plasmon hybrids. The exciton and plasmon damping coefficients γ^{ex} , γ^{pl} and γ_o^{ex} are temperature dependent, cp. Eqs. (4,9,24). Therefore, we obtain qualitatively different spectra for different temperatures.

2. Scattering Cross Section

The momentum-dark excitons correspond to a localized exciton distribution under the MNP with extensions small compared to the wavelength of the incident light [94]. Therefore, the scattering cross section of the hybridized exciton-plasmon system can be modeled based on the scattering cross section of a point dipole [95]

$$S_{\text{scat}} = \frac{1}{6\pi\epsilon_0^2} \frac{\omega^4}{c^4} |\alpha^{\text{plex}}(\omega)|^2 \quad (72)$$

with the polarizability α^{plex} that in this case is a coupled plasmon-exciton polarizability. It connects the resulting dipole with the incident field and is therefore defined by the comparison of

$$\mathbf{p}^{\text{pl}}(t) = \alpha^{\text{plex}}(\omega) \mathbf{E}^0(t) \quad (73)$$

with the solution for the plasmon dynamics in the hybrid system, cp. Eq. (58). Equations (72 and 73) are only defined in the complex representation of electrodynamics where the polarizability is given by

$$\alpha^{\text{plex}}(\omega) = \frac{-\left(\omega^2 + i\omega\gamma^{\text{ex}} - \omega_{\text{ex}\bullet}^2\right) f^{\text{pl}}}{\left(\omega^2 + i\omega\gamma^{\text{pl}} - \omega_{\text{isp}}^2\right) \left(\omega^2 + i\omega\gamma^{\text{ex}} - \omega_{\text{ex}\bullet}^2\right) - g^{\text{pl}}g_{\bullet}^{\text{ex}}} \quad (74)$$

Thus we find for the scattering cross section:

Scattering Cross Section	(75)
$S_{\text{scat}} = \frac{ f^{\text{pl}} ^2 \omega^4}{6\pi\epsilon_0^2 c^4} \left \frac{\left(\omega^2 + i\omega\gamma^{\text{ex}} - \omega_{\text{ex}\bullet}^2\right)}{\left(\omega^2 + i\omega\gamma^{\text{pl}} - \omega_{\text{isp}}^2\right) \left(\omega^2 + i\omega\gamma^{\text{ex}} - \omega_{\text{ex}\bullet}^2\right) - g^{\text{pl}}g_{\bullet}^{\text{ex}}} \right ^2$	

The translation-invariant, homogeneous distribution of bright excitons in the 2d TMDC does not contribute to the scattering as measured in dark-field spectroscopy but only to reflection and transmission perpendicular to the TMDC plane. Thus, we would not expect the bright excitonic mode to be visible in dark-field measurements.

IV. RESULTS

To put the results of the three coupled oscillator model (3-COM) into the context of the known model of two coupled oscillators we first discuss two undamped, harmonic oscillators in strict resonance: In this ideal case, the estimated mode-splitting Ω_g follows the coupling constant via [33]

$$\Omega_g = \hbar \frac{g_{\text{eff}}}{\omega_{\text{isp}}} \quad (76)$$

Whether the mode splitting manifests as a peak splitting in optical spectra depends on its ratio to the spectral linewidths, that is, the damping coefficients of the individual oscillators. The hybrid system is assigned to weak coupling if the mode splitting is smaller than the mean damping coefficient, $\Omega_g < (\gamma^{\text{ex}} + \gamma^{\text{pl}})/2$, and to strong coupling if it is larger, $\Omega_g > (\gamma^{\text{ex}} + \gamma^{\text{pl}})/2$.

The parameters used in this entire section are provided in table II. The temperature-dependent damping coefficients are depicted in Fig. 4, where the mean value is compared with the estimated mode splitting Ω_g for different distances $\delta z \in \{12, 17, 30\}$ nm between the TMDC layer and MNP

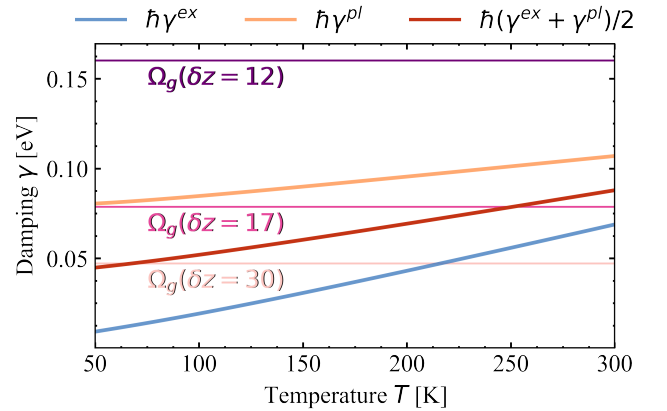


Figure 4. Comparison of mode splittings Ω_g (thin horizontal lines) for different exciton-plasmon distances δz with the temperature-dependent damping of momentum-dark exciton γ^{ex} (blue), plasmon $\gamma^{\text{pl}}(T)$ (orange) and with their mean value (red).

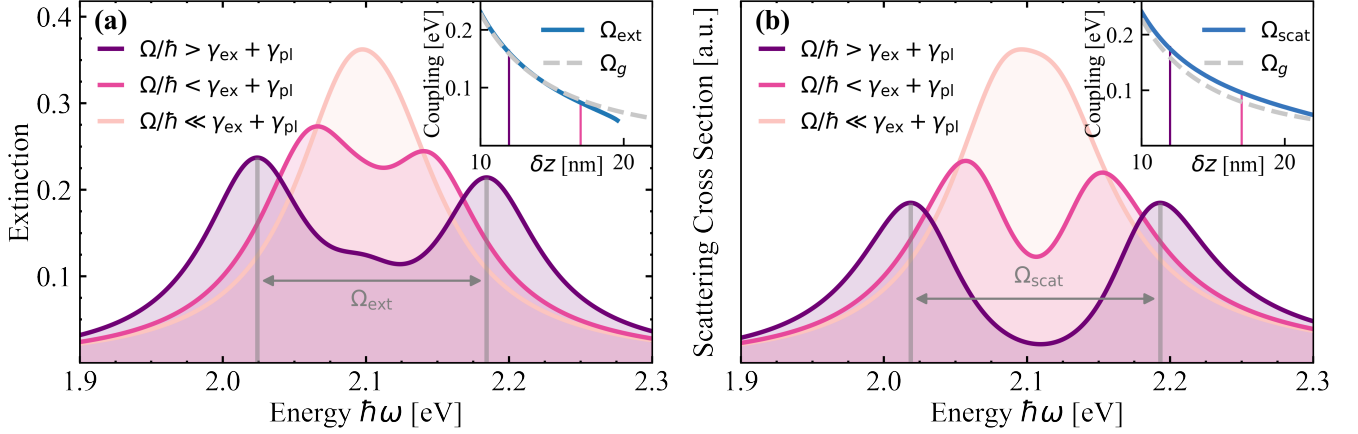


Figure 5. (a) Extinction / (b) Scattering cross section for different distances $\delta z = \{12, 17, 30\}$ nm between the TMDC and the MNP at room temperature $T = 293$ K. The figure shows the distance dependence of exciton-plasmon coupling and its influence on the line shape, that is, a transition from weak coupling (large distances) to strong coupling (small distances). Insets: Comparison between the distance dependency of the coupling constant ($\sim \Omega_g$) and the peak splitting extracted from the respective spectrum (a) Ω_{ext} and (b) Ω_{scat} . For weak coupling strengths the peak splitting vanishes which is extinction at $\delta z \gtrsim 20$ nm.

center, cp. Fig. 1. For small distances ($\delta z = 12$ nm), the estimated mode splitting Ω_g remains in the strong coupling regime across the entire temperature range $T \in [50, 300]$, lying well above the mean damping coefficient. At larger distances, the system shifts to the weak coupling regime.

We now turn to the resulting optical spectra. Figures 5a and 5b show extinction, Eqs. (70,71), and scattering, Eq. (75), at room temperature for the different distances δz . These spectra show the transition from weak coupling at larger distances, e.g., $\delta z = 30$ nm, to strong coupling at smaller distances, comparable to the extensions of the MNP (e.g., $\delta z = 12$ nm $\gtrsim r_z$).

The insets in Figs. 5a and 5b compare the distance dependence of the estimated mode splitting Ω_g with the peak splitting extracted from the respective spectrum ($\Omega_{\text{ext/scat}}$). For extinction, Fig. 5a, there is a very good agreement between Ω_{ext} and Ω_g in the strong coupling regime. However, in scattering, Fig. 5b, Ω_{scat} deviates from Ω_g . The reason for this deviation is the ω^4 prefactor of the dipole scattering efficiency, cp. Eq. (75).

Furthermore, the extinction spectrum in fig. 5a differs in another aspect from the ideal case: For two perfectly resonant oscillators, the amplitude of the hybridized modes in extinction spectra would be exactly equal. In our case, despite setting $\omega_{\text{isp}} = \omega_{\text{exo}}$, we observe a slight asymmetry between the two peaks. The asymmetry arises because the plasmon is resonant with the bright exciton mode but not with the momentum-dark excitons, which are strongly coupled but lie at higher energies. Since the light-matter interaction of the momentum-dark excitons is mediated by the plasmon, the lower energy mode, which has more plasmonic character when the plasmon resonance frequency is lower than the momentum-dark exciton, is more pronounced. In fact, the 3-COM underestimates this asymmetry by summarizing the continuum of momentum-dark energy states in one effective mode. A semi-analytical study without this approximation, necessitating a

Table II. Material parameters for TMDC and MNP

Parameter	Value	Unit	Reference
d	0.25	e nm	[75]
M	6.1	eV fs ² nm ⁻²	[70]
c_1	0.182	meV K ⁻¹	[73]
c_2	15.6 31.2	meV	[73]
Ω	30	meV	[73]
φ_0	0.46	nm ⁻¹	a
ε_∞	1.53		[85]
$\omega_{\text{pl,bulk}}$	12.99	fs ⁻¹	[85]
ω_1	4.02	fs ⁻¹	[85]
ω_2	5.69	fs ⁻¹	[85]
Γ_1	0.82	fs ⁻¹	[85]
Γ_2	2.00	fs ⁻¹	[85]
A_1	0.94		[85]
A_2	1.36		[85]
ϕ_1	$-\pi/4$		[85]
ϕ_2	$-\pi/4$		[85]
b	0.6329	eV ⁻¹	[90]
γ_0	0.0219	eV	[90]
Θ	185	K	[90]
c	299.7925	nm fs ⁻¹	
ε_0	0.05526308	e ² eV ⁻¹ nm ⁻¹	
\hbar	0.658212196	eV fs	
k_B	0.0861745	meV K ⁻¹	
r_x	30	nm	
r_y	30	nm	
r_z	10	nm	
δz	12	nm	
ε_{out}	3		
A	16000	nm ²	

^a appears as the solution of the Wannier equation, similar to Refs. [104, 105], for the chosen dielectric environment.

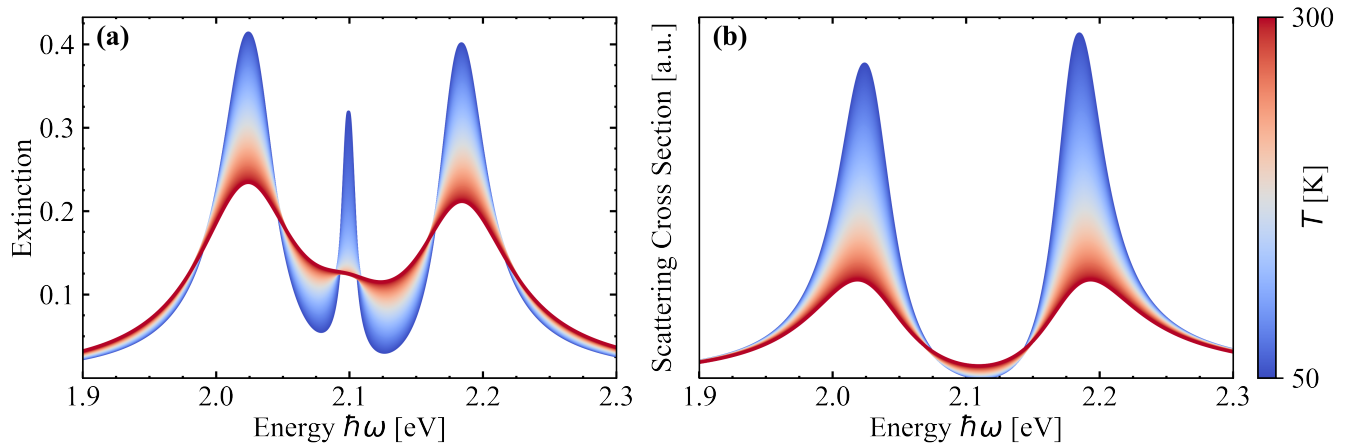


Figure 6. Spectra for different temperatures T . (a) Extinction: at high temperatures, the spectrum resembles almost a typical strong coupling spectrum of two coupled oscillators, with the higher energy peak showing a slightly reduced amplitude due to the detuning between the plasmon and the collective momentum-dark exciton mode. The additional bright exciton peak becomes more pronounced at lower temperatures. (b) Scattering cross section: It includes only the scattering at the MNP plasmon, influenced by the coupling to the TMDC excitons, displaying typical strong coupling characteristics.

numerical evaluation, is conducted in Ref. 66. For the scattering cross section, an asymmetry between the modes is characteristic due to the ω^4 dependence even in the perfectly resonant case, making the high-energy mode more pronounced. This effect counteracts the asymmetry caused by the effective detuning of the hybridized oscillators.

For extinction, the strong coupling case in Fig. 5a hints to the emergence of a third, central peak. To better resolve this feature, Figs. 6a and 6b show the extinction and scattering spectra, respectively, for varying temperatures. In the model, the temperature influences both the exciton and plasmon damping coefficients, leading to qualitatively different spectra. At room temperature, the spectra exhibit the typical strong coupling characteristics of two coupled oscillators. As the temperature decreases, an additional central peak becomes visible in the extinction because the reduced damping allows for a clear observation of the bright exciton mode. In contrast, the delocalized bright excitons have no contribution to the scattering cross section, according to the model in Sec. III E 2, and thus can not be observed in dark-field measurements.

According to Eq. (70), the ratio of the hybridized plasmon-dark exciton modes and the bright exciton contribution to the extinction depends on both temperature T and the illuminated area A of the TMDC per MNP. In samples with multiple MNPs (assuming no interactions between them), this parameter corresponds to the inverse of the MNP density. The assumption of negligible interactions between MNPs is valid for randomly distributed MNPs and a certain range of distances ($\sim 3r_x$) [15, 66, 106]. We evaluate the extinction for varying $A \in [0.16, 1] \mu\text{m}^2$ at liquid nitrogen temperature in Fig. 7. For a laser spot size $A = 0.16 \mu\text{m}^2$ right at the diffraction limit with a single MNP on the TMDC, the spectrum is dominated by hybridized plasmon - dark exciton modes. With increasing A , the bright exciton mode becomes more pronounced.

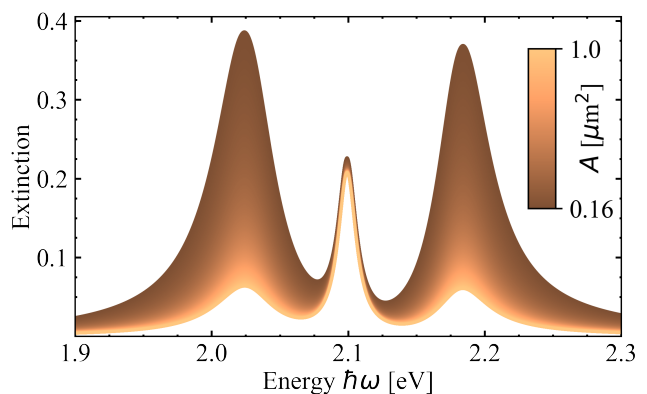


Figure 7. Extinction for different sizes of the illuminated area A per MNP at liquid nitrogen temperature $T = 77 \text{ K}$. The larger the illuminated area of the TMDC per MNP, the more pronounced is the middle, bright exciton in relation to the hybridized plasmon - dark exciton modes.

V. CONCLUSION

We developed a modified three coupled oscillator model (3-COM) to describe experimentally accessible observables, such as extinction and scattering, in hybrid systems composed of metal nanoparticles (MNPs) and two-dimensional delocalized excitons, e.g., in transition metal dichalcogenides (TMDCs). For the occurring coupling parameters we provide explicit expressions depending on distance of MNP and TMDC, MNP number density, MNP volume and shape as well as material properties. Most importantly, the 3-COM incorporates key extensions to the conventional COM by accounting for the spatial delocalization of two-dimensional excitons, distinguishing between bright and momentum-dark exciton

modes, and their interactions with MNP plasmons.

We have demonstrated that while bright excitons remain weakly coupled, momentum-dark excitons can exhibit strong coupling with MNP plasmons but lie at higher energies. This results in the appearance of a distinct third (bright exciton) peak in the optical spectra [101] and an asymmetry between the hybridized plasmon-dark exciton modes [6, 51, 54, 56–59], consistent with experimental observations.

The visibility of the bright exciton mode in the hybrid spectrum is determined by temperature and MNP density, though it is not observable in dark-field spectra, which only detect scattered light.

While the simplified 3-COM offers significant advantages, particularly in its ability to fit experimental data, it involves certain approximations. The assumption that the MNP plasmon fully covers the absorption (e.g., Drude susceptibility) excludes possible contributions from inner metal bands, limiting the model to a certain frequency range and reducing its ability to fully account for the impact of surrounding permittivity. On the exciton side, the effective treatment of momentum-dark excitons as a single mode simplifies the model but underestimates the resulting asymmetry in the hybridized modes [66, 94], as a continuum of excitonic energy states is compressed into one representative energy level. This simplification also leads to an overestimation of the coupling constant, that, however, is no limitation for the application of this model for fitting experimental spectra.

In summary, our analytical approach bridges the gap between traditional phenomenological models [32–35] and rigorous microscopic theory [66, 94, 107, 108] for TMDC-MNP hybrid systems. It offers a straightforward and physically grounded framework for fitting and interpreting experimental results in nanoscale optical systems using Eqs. (71 and 75), which together with the derived oscillator model, Eq. (56), constitute the main result of our work.

VI. ACKNOWLEDGMENTS

We would like to thank Jonas Grumm, Robert Fuchs, Joris Sturm, Frank Jahnke and David Greten for their insightful comments on various topics related to this work. Further, we acknowledge the assistance of generative AI (ChatGPT) in improving the language clarity of this manuscript.

Appendix A: Fourier transform

The Fourier transform regarding the in-plane spatial coordinates $\mathbf{r}_{\parallel} = (x, y)^T$ and its inverse for an arbitrary scalar or vector function \mathbf{f} are given by:

$$\mathbf{f}(\mathbf{r}) = \frac{1}{(2\pi)^2} \int d^2\mathbf{q}_{\parallel} e^{i\mathbf{q}_{\parallel} \cdot \mathbf{r}} \mathbf{f}(\mathbf{q}_{\parallel}, z) \quad (\text{A1})$$

$$\mathbf{f}(\mathbf{q}_{\parallel}, z) = \int d^2\mathbf{r}_{\parallel} e^{-i\mathbf{q}_{\parallel} \cdot \mathbf{r}} \mathbf{f}(\mathbf{r}) \quad (\text{A2})$$

The Fourier transform with respect to time is defined with opposite sign in the exponential compared to the spatial transformation.

$$\mathbf{f}(t) = \frac{1}{2\pi} \int d\omega e^{-i\omega t} \mathbf{f}(\omega) \quad (\text{A3})$$

$$\mathbf{f}(\omega) = \int dt e^{i\omega t} \mathbf{f}(t) \quad (\text{A4})$$

Appendix B: Reduction from 3 to 2 dimensions

In the main text, we state that it is sufficient to treat the in-plane directions of the MNP dipole and the TMDC dipole density, dropping their z -entries. From this follows that also the description of the resulting electric fields and so the effective Green's dyadic simplifies significantly. Here, we provide a proof for this statement.

In the developed theory, we need the Green's dyadic twice: 1. To determine the electric field emitted by the TMDC excitons, observed at the position of the MNP

$$\mathbf{E}^{\text{ex}}(\mathbf{r}_{\text{pl}}; \omega) = \frac{1}{(2\pi)^2} \int d^2q_{\parallel} \mathcal{G}_{\mathbf{q}_{\parallel}}(z_{\text{pl}}, z_{\text{ex}}; \omega) \cdot \mathbf{P}_{\mathbf{q}_{\parallel}}^{\text{ex}}(\omega) \quad (\text{B1})$$

and 2. vice versa, the electric field emitted by the MNP plasmon, observed in the TMDC monolayer

$$\mathbf{E}_{\mathbf{q}_{\parallel}}^{\text{pl}}(z_{\text{ex}}; \omega) = \mathcal{G}_{\mathbf{q}_{\parallel}}(z_{\text{ex}}, z_{\text{pl}}; \omega) \cdot \mathbf{P}^{\text{pl}}(\omega). \quad (\text{B2})$$

The full 3×3 Green's dyadic (in-plane Fourier transformed) is given by

$$\mathcal{G}_{\mathbf{q}_{\parallel}}(z, z', \omega) = \begin{pmatrix} -\frac{\omega^2}{\epsilon_0 c^2} \mathbb{1} + \frac{\mathbf{q}_{\parallel} \otimes \mathbf{q}_{\parallel}}{\epsilon_0 \epsilon_{\text{out}}} & \frac{i\mathbf{q}_{\parallel}}{\epsilon_0 \epsilon_{\text{out}}} \partial_{z'} \\ \frac{i\mathbf{q}_{\parallel}^T}{\epsilon_0 \epsilon_{\text{out}}} \partial_{z'} & -\frac{\omega^2}{\epsilon_0 c^2} - \frac{1}{\epsilon_0 \epsilon_{\text{out}}} \partial_{z'}^2 \end{pmatrix} G_{\mathbf{q}_{\parallel}}(z, z', \omega). \quad (\text{B3})$$

We now step by step drop components of the Green's dyadic, Eq. (B3), that are not necessary to represent Eqs. (B1 and B2).

Due to the in-plane orientation of the TMDC exciton dipole moment, we first know that the exciton dipole density has a negligible z -entry.

$$\mathbf{P}_{\mathbf{q}_{\parallel}}^{\text{ex}}(\omega) = \begin{pmatrix} P_{\mathbf{q}_{\parallel}x}^{\text{ex}} \\ P_{\mathbf{q}_{\parallel}y}^{\text{ex}} \\ 0 \end{pmatrix} \quad (\text{B4})$$

By representing $\mathbf{P}_{\mathbf{q}_{\parallel}}^{\text{ex}}$ as a 2-dimensional vector in Eq. (B1), the Green's dyadic there effectively reduces to 3×2 . Second, to determine the exciton dynamics we need $\mathbf{d}^{\xi} \cdot \mathbf{E}_{\mathbf{q}_{\parallel}}^{\text{pl}}$ which does not depend on the z -component of the electric field. Therefore, there is no need to calculate the z -entry of $\mathbf{E}_{\mathbf{q}_{\parallel}}^{\text{pl}}$, allowing to reduce the dimensions of the Green's dyadic in Eq. (B2) to 2×3 .

To get rid of the remaining z -entries, we start with the ansatz, that also the MNP dipole has a vanishing z -entry

$$\mathbf{p}^{\text{pl}}(\omega) = \begin{pmatrix} p_x^{\text{pl}} \\ p_y^{\text{pl}} \\ 0 \end{pmatrix}, \quad (\text{B5})$$

which is not yet proven to self-consistently solve the exciton-plasmon coupling dynamics. However, if this assumption is valid, the dimensions of Eqs. (B1) and (B2) may be reduced to 2×2 (similar arguments as above). Thus, we finally have to show that from an initially in-plane oriented MNP dipole, excited by the in-plane oriented incident electric field, the coupling to the TMDC acts in such a way, that its back-action does not excite the z -component of the MNP dipole. Following the definition of the polarizability

$$\mathbf{p}^{\text{pl}}(\omega) = \boldsymbol{\alpha}(\omega) \cdot \mathbf{E}(\mathbf{r}_{\text{pl}}, \omega) \quad (\text{B6})$$

with $\boldsymbol{\alpha}$ being diagonal in a Cartesian basis, it follows that $p_z^{\text{pl}} = 0$ if and only if $E_z(\mathbf{r}_{\text{pl}}; \omega) = E_z^0(\mathbf{r}_{\text{pl}}; \omega) + E_z^{\text{ex}}(\mathbf{r}_{\text{pl}}; \omega) = 0$. Since we only consider an incoming electric field \mathbf{E}^0 with in-plane orientation, $E_z^0(\mathbf{r}_{\text{pl}}; \omega) = 0$ is valid. The z -entry of the electric field emitted by the excitons can be determined using Eq. (B1). The z -row of the remained 3×2 Green's dyadic, Eq. (B3), is odd in $q_{\parallel x}$ and $q_{\parallel y}$ since the scalar Green's function only depends on $q_{\parallel} = |\mathbf{q}_{\parallel}|$. Thus, the relevant \mathbf{q}_{\parallel} integral vanishes and $E_z^{\text{ex}}(\mathbf{r}_{\text{pl}}; \omega) = 0$ is valid, if all entries of the exciton dipole density $\mathbf{P}_{\mathbf{q}_{\parallel}}^{\text{ex}}$ are even, which in fact is fulfilled if $p_z^{\text{pl}} = 0$. In summary, the ansatz, Eq. (B6), self-consistently solves the coupled light-matter respectively exciton-plasmon dynamics, and may be described effectively using only 2d dipole densities without any further approximation.

Appendix C: Energy balance

In this Appendix, we evaluate the energy balance for the MNP-TMDC hybrid under illumination with the incident electric field \mathbf{E}^0 to find an expression for the extinction: The total absorbed energy is

$$W_{\text{abs}} = \int_{\tau} dt \int_V d^3r \mathbf{E}(\mathbf{r}, t) \cdot \dot{\mathbf{P}}(\mathbf{r}, t). \quad (\text{C1})$$

In our case, the full electric field is given by

$$\mathbf{E}(\mathbf{r}; t) = \mathbf{E}^{\text{ex}^\circ}(\mathbf{r}; t) + \mathbf{E}^{\text{ex}^\bullet}(\mathbf{r}; t) + \mathbf{E}^{\text{pl}}(\mathbf{r}; t) + \mathbf{E}^0(\mathbf{r}; t) \quad (\text{C2})$$

and the full dipole density by

$$\mathbf{P}(\mathbf{r}; t) = \mathbf{P}^{\text{ex}^\circ}(\mathbf{r}; t) + \mathbf{P}^{\text{ex}^\bullet}(\mathbf{r}; t) + \mathbf{P}^{\text{pl}}(\mathbf{r}; t) \quad (\text{C3})$$

with the TMDC dipole density in thin film approximation and the MNP reduced to a point dipole:

$$\mathbf{P}^{\text{ex}^\circ}(\mathbf{r}; t) = \mathbf{P}^{\text{ex}^\circ}(\mathbf{r}_{\parallel}; t) \delta(z - z_{\text{ex}}) \quad (\text{C4})$$

$$\mathbf{P}^{\text{ex}^\bullet}(\mathbf{r}; t) = \mathbf{P}^{\text{ex}^\bullet}(\mathbf{r}_{\parallel}; t) \delta(z - z_{\text{ex}}) \quad (\text{C5})$$

$$\mathbf{P}^{\text{pl}}(\mathbf{r}; t) = \mathbf{p}^{\text{pl}}(t) \delta(\mathbf{r} - \mathbf{r}^{\text{pl}}) \quad (\text{C6})$$

Taking into account Eqs. (C2,C3), the total absorbed energy, Eq. (C1), can be divided into the following contributions

$$W_{\text{abs}} = W^{\text{ex}^\bullet \leftrightarrow \text{pl}} + W^{\text{ex}^\circ \leftrightarrow \text{pl}} + W^{\text{ex}^\circ \leftrightarrow \text{ex}^\bullet} \quad (\text{C7}) \\ + W^{\text{ex}^\circ, \text{rad}} + W^{\text{ex}^\bullet, \text{rad}} + W^{\text{pl}, \text{rad}} + W^0.$$

The individual terms are:

1. The work done by the plasmon on the dark exciton distribution plus vice versa

$$W^{\text{ex}^\bullet \leftrightarrow \text{pl}} = \int_{\tau} dt \int_V d^3r \mathbf{E}^{\text{pl}}(\mathbf{r}, t) \cdot \partial_t \mathbf{P}^{\text{ex}^\bullet}(\mathbf{r}; t) \quad (\text{C8}) \\ + \int_{\tau} dt \int_V d^3r \mathbf{E}^{\text{ex}^\bullet}(\mathbf{r}, t) \cdot \partial_t \mathbf{P}^{\text{pl}}(\mathbf{r}, t) = 0.$$

It vanishes due to energy conservation, since the work done by the plasmon on the dark exciton distribution is in turn received by the excitons. We prove the relation in Sec. C1.

2. We disregard the energy exchange between bright exciton and plasmon here by stating

$$W^{\text{ex}^\circ \leftrightarrow \text{pl}} = \int_{\tau} dt \int_V d^3r \mathbf{E}^{\text{pl}}(\mathbf{r}, t) \cdot \partial_t \mathbf{P}^{\text{ex}^\circ}(\mathbf{r}; t) \quad (\text{C9}) \\ + \int_{\tau} dt \int_V d^3r \mathbf{E}^{\text{ex}^\circ}(\mathbf{r}, t) \cdot \partial_t \mathbf{P}^{\text{pl}}(\mathbf{r}, t) = 0,$$

to stay consistent with the approximations of the main paper, where we neglect the corresponding minor interaction.

3. The energy exchange between bright and dark excitons vanishes,

$$W^{\text{ex}^\circ \leftrightarrow \text{ex}^\bullet} = \int_{\tau} dt \int_V d^3r \mathbf{E}^{\text{ex}^\bullet}(\mathbf{r}, t) \cdot \partial_t \mathbf{P}^{\text{ex}^\circ}(\mathbf{r}; t) \quad (\text{C10}) \\ + \int_{\tau} dt \int_V d^3r \mathbf{E}^{\text{ex}^\circ}(\mathbf{r}, t) \cdot \partial_t \mathbf{P}^{\text{ex}^\bullet}(\mathbf{r}, t) = 0,$$

since they do not interact (see Sec. C2).

4. The out-going (radiated), respectively scattered energy

$$W_{\text{rad}} = W^{\text{ex}^\bullet, \text{rad}} + W^{\text{ex}^\circ, \text{rad}} + W^{\text{pl}, \text{rad}} \quad (\text{C11})$$

with the contributions

$$W^{\text{ex}^\circ, \text{rad}} = \int_{\tau} dt \int_V d^3r \mathbf{E}^{\text{ex}^\circ}(\mathbf{r}, t) \cdot \partial_t \mathbf{P}^{\text{ex}^\circ}(\mathbf{r}; t), \quad (\text{C12})$$

$$W^{\text{ex}^\bullet, \text{rad}} = \int_{\tau} dt \int_V d^3r \mathbf{E}^{\text{ex}^\bullet}(\mathbf{r}, t) \cdot \partial_t \mathbf{P}^{\text{ex}^\bullet}(\mathbf{r}; t), \quad (\text{C13})$$

$$W^{\text{pl}, \text{rad}} = \int_{\tau} dt \int_V d^3r \mathbf{E}^{\text{pl}}(\mathbf{r}, t) \cdot \partial_t \mathbf{P}^{\text{pl}}(\mathbf{r}; t), \quad (\text{C14})$$

is dealt with in Sec. C3.

5. The work done by the incident electric field on the dipole density distribution

$$W^0 = \int_{\tau} dt \int_V d^3r \mathbf{E}^0(\mathbf{r}, t) \cdot \dot{\mathbf{P}}(\mathbf{r}, t). \quad (\text{C15})$$

is dealt with in Sec. C 4. Since the remaining terms of the energy balance, Eq. (C7), are

$$W_{\text{abs}} = W^0 + W_{\text{rad}} \quad (\text{C16})$$

and extinction is by definition the sum of absorption and scattered/re-radiated energy

$$W_{\text{ext}} = W_{\text{abs}} - W_{\text{rad}} \quad (\text{C17})$$

with $W_{\text{rad}} < 0$, we find that the work done by the incident electric field on the full dipole density corresponds to extinction

$$W^0 = W_{\text{ext}}. \quad (\text{C18})$$

Since the scattering / radiated energy W_{rad} is included, the quantity $W^0 = W_{\text{ext}}$ is typically larger than the true absorption W_{abs} .

In the explicit evaluation of all terms for the hybrid TMDC-MNP geometry, we have to take care, that the approximations are consistent with the approximations made in the main paper.

1. $W^{\text{ex} \leftrightarrow \text{pl}}$: plasmon - dark exciton quasi-static energy exchange

We consider two exemplary dipole density distributions $\mathbf{P}^1(\mathbf{r}; t)$ and $\mathbf{P}^2(\mathbf{r}; t)$ that interact via the electric near-field in quasi-static approximation and may correspond to the MNP plasmon $\mathbf{P}^{\text{pl}}(\mathbf{r}, t)$ and TMDC dark exciton $\mathbf{P}^{\text{ex} \bullet}(\mathbf{r}, t)$ dipole density. The electro-magnetic fields $\mathbf{E}^l, \mathbf{B}^l$ with $l \in \{1, 2\}$ generated by these distributions individually obey Maxwell's equations. Thus

$$\nabla \times \mathbf{B}^l = \mu_0 \partial_t \mathbf{P}^l + \mu_0 \varepsilon_0 \varepsilon \partial_t \mathbf{E}^l. \quad (\text{C19})$$

We multiply Eq. (C19) from the left with $\mathbf{E}^{\bar{l}}$ where $l \neq \bar{l} \in \{1, 2\}$ and add the two resulting equations.

$$\begin{aligned} \mathbf{E}^2 \cdot (\nabla \times \mathbf{B}^1) + \mathbf{E}^1 \cdot (\nabla \times \mathbf{B}^2) = & \quad (\text{C20}) \\ \mu_0 \mathbf{E}^2 \cdot \partial_t \mathbf{P}^1 + \mu_0 \mathbf{E}^1 \cdot \partial_t \mathbf{P}^2 & \\ + \mu_0 \varepsilon_0 \varepsilon \mathbf{E}^2 \cdot \partial_t \mathbf{E}^1 + \mu_0 \varepsilon_0 \varepsilon \mathbf{E}^1 \cdot \partial_t \mathbf{E}^2. & \end{aligned}$$

Integrating over a sufficiently large volume V and an oscillation period $\tau = \frac{2\pi}{\omega}$ yields

$$\begin{aligned} \int_{\tau} dt \int_V d^3r (\mathbf{E}^2 \cdot (\nabla \times \mathbf{B}^1) + \mathbf{E}^1 \cdot (\nabla \times \mathbf{B}^2)) & \quad (\text{C21}) \\ = \int_{\tau} dt \int_V d^3r (\mu_0 \mathbf{E}^2 \cdot \partial_t \mathbf{P}^1 + \mu_0 \mathbf{E}^1 \cdot \partial_t \mathbf{P}^2) & \\ + \int_{\tau} dt \int_V d^3r (\mu_0 \varepsilon_0 \varepsilon \mathbf{E}^2 \cdot \partial_t \mathbf{E}^1 + \mu_0 \varepsilon_0 \varepsilon \mathbf{E}^1 \cdot \partial_t \mathbf{E}^2). & \end{aligned}$$

First, we treat the first line of Eq. (C21). We find

$$\begin{aligned} \mathbf{E}^2 \cdot (\nabla \times \mathbf{B}^1) + \mathbf{E}^1 \cdot (\nabla \times \mathbf{B}^2) & \quad (\text{C22}) \\ = \nabla \cdot (\mathbf{E}^2 \times \mathbf{B}^1 + \mathbf{E}^1 \times \mathbf{B}^2), & \end{aligned}$$

where we used that the curl $\nabla \times \mathbf{E}^l$ vanishes, since these electric fields have been treated in the quasi-static limit in the main paper and therefore are pure gradient fields. Following Gauss' theorem, the divergence allows to transform the integral over the volume V to an integral over the boundary area ∂V . We choose V to be large, such that ∂V is sufficiently far away and the integral vanishes, since the electric near-fields \mathbf{E}^1 and \mathbf{E}^2 decrease exponentially with the distance. Therefore, we find

$$\int_{\tau} dt \int_V d^3r (\mathbf{E}^2 \cdot (\nabla \times \mathbf{B}^1) + \mathbf{E}^1 \cdot (\nabla \times \mathbf{B}^2)) = 0. \quad (\text{C23})$$

Next, we turn our attention to the last line of Eq. (C21). In our case, the electric fields are monochromatic with the frequency ω . The time dependency of the electric fields is therefore generally given by

$$\mathbf{E}^l \sim \cos(\omega t - \varphi^l) \quad (\text{C24})$$

with the individual phase shift φ^l . We further define the abbreviation $\varphi^1 - \varphi^2 = \delta\varphi$. It follows that

$$\begin{aligned} \int_{\tau} dt (\mathbf{E}^2 \cdot \partial_t \mathbf{E}^1 + \mathbf{E}^1 \cdot \partial_t \mathbf{E}^2) & \quad (\text{C25}) \\ \sim \int_{\tau} dt (\cos(\omega t) \sin(\omega t + \delta\varphi) + \cos(\omega t + \delta\varphi) \sin(\omega t)) & \\ = \int_{\tau} dt \sin(2\omega t + \delta\varphi) & \\ = 0 & \end{aligned}$$

vanishes since $\tau = \frac{2\pi}{\omega}$. Therefore, from Eq. (C21), it follows

$$W^{1 \leftrightarrow 2} = \int_{\tau} dt \int_V d^3r (\mu_0 \mathbf{E}^2 \cdot \partial_t \mathbf{P}^1 + \mu_0 \mathbf{E}^1 \cdot \partial_t \mathbf{P}^2) = 0, \quad (\text{C26})$$

All assumptions made in this derivation for the distributions 1 and 2 are valid for the MNP plasmon and TMDC momentum dark exciton distribution. Therefore, we deduce

$$W^{\text{ex} \bullet \leftrightarrow \text{pl}} = 0. \quad (\text{C27})$$

2. $W^{\text{ex} \circ \leftrightarrow \text{ex} \bullet}$: bright exciton - dark exciton energy exchange

The energy exchange between bright and dark excitons is given by

$$\begin{aligned} W^{\text{ex} \circ \leftrightarrow \text{ex} \bullet} = \int_{\tau} dt \int_A d^2r_{\parallel} \mathbf{E}^{\text{ex} \bullet}(\mathbf{r}_{\parallel}, z_{\text{ex}}, t) \cdot \partial_t \mathbf{P}^{\text{ex} \circ}(\mathbf{r}_{\parallel}; t) & \quad (\text{C28}) \\ + \int_{\tau} dt \int_A d^2r_{\parallel} \mathbf{E}^{\text{ex} \circ}(\mathbf{r}_{\parallel}, z_{\text{ex}}, t) \cdot \partial_t \mathbf{P}^{\text{ex} \bullet}(\mathbf{r}_{\parallel}; t), & \end{aligned}$$

where the 3d integral over the volume V reduces to 2d over the area A due to the thin film approximation for the exciton dipole densities, cp. Eqs. (C4,C5). The bright exciton dipole density respectively its emitted electric field (stemming from the $q_{\parallel} = 0$ mode) are constant regarding the in-plane coordinate and therefore regarding the spatial integral over \mathbf{r}_{\parallel} . For the dark exciton dipole density or its emitted electric field, the spatial integral can then be interpreted as a Fourier-transform, evaluated at $\mathbf{q}_{\parallel} = 0$. This yields

$$W^{\text{ex}\circ \leftrightarrow \text{ex}\bullet} = \int_{\tau} dt \mathbf{E}_{\mathbf{q}_{\parallel}=0}^{\text{ex}\bullet}(z_{\text{ex}}, t) \cdot \partial_t \mathbf{P}^{\text{ex}\circ}(\mathbf{r}_{\parallel}; t) \quad (\text{C29})$$

$$+ \int_{\tau} dt \mathbf{E}^{\text{ex}\circ}(\mathbf{r}_{\parallel}, z_{\text{ex}}, t) \cdot \partial_t \mathbf{P}_{\mathbf{q}_{\parallel}=0}^{\text{ex}\bullet}(t).$$

As discussed in the main paper, the dark exciton distribution and its emitted electric field vanish at $\mathbf{q}_{\parallel} = 0$. It follows

$$W^{\text{ex}\circ \leftrightarrow \text{ex}\bullet} = 0, \quad (\text{C30})$$

which is physically intuitive since we found no electric field mediated interactions at all between bright and momentum dark excitons in the main paper.

3. W_{rad} : radiated/scattered energy

The light emitted by the hybrid system carries the energy

$$W_{\text{rad}} = W_{\text{rad}}^{\text{ex}\bullet} + W_{\text{rad}}^{\text{ex}\circ} + W_{\text{rad}}^{\text{pl}}. \quad (\text{C31})$$

The individual energy radiatively lost by a dipole density distribution \mathbf{P}^j , $j \in \{\text{ex}\bullet, \text{ex}\circ, \text{pl}\}$, is given by

$$W_{\text{rad}}^j = \int_{\tau} dt \int_V d^3r \mathbf{E}^j(\mathbf{r}, t) \cdot \partial_t \mathbf{P}^j(\mathbf{r}, t). \quad (\text{C32})$$

For $j = \text{ex}\bullet$, we insert the emitted electric field via the dyadic Green's function in quasi-static approximation

$$\mathbf{E}^{\text{ex}\bullet}(\mathbf{r}, t) = \int_V d^3r' \underline{\mathcal{G}}(\mathbf{r} - \mathbf{r}') \cdot \mathbf{P}^{\text{ex}\bullet}(\mathbf{r}', t) \quad (\text{C33})$$

and the separation ansatz, which corresponds to the separation ansatz in the main paper but in real space,

$$\mathbf{P}^{\text{ex}\bullet}(\mathbf{r}, t) = P^{\text{ex}\bullet}(\mathbf{r}) P^{\text{ex}\bullet}(t) \mathbf{e}_P. \quad (\text{C34})$$

with the unit vector \mathbf{e}_P . Thus, we find:

$$W_{\text{rad}}^{\text{ex}\bullet} = \int_{\tau} dt P^{\text{ex}\bullet}(t) \partial_t P^{\text{ex}\bullet}(t) \quad (\text{C35})$$

$$\int_V d^3r \left(\int_V d^3r' \underline{\mathcal{G}}(\mathbf{r} - \mathbf{r}') \cdot P^{\text{ex}\bullet}(\mathbf{r}') \mathbf{e}_P \right) \cdot P^{\text{ex}\bullet}(\mathbf{r}) \mathbf{e}_P$$

The time dependence is $P^{\text{ex}\bullet}(t) \sim \cos(\omega t + \varphi^{\text{ex}\bullet})$. Therefore, the integral over the time period τ vanishes and we find

$$W_{\text{rad}}^{\text{ex}\bullet} = 0, \quad (\text{C36})$$

which is reasonable since the dark excitons do not directly emit radiation.

The bright exciton dipole distribution and its emitted electric field are constant regarding the in-plane coordinate \mathbf{r}_{\parallel} . With Eq. (C4), we find

$$W_{\text{rad}}^{\text{ex}\circ} = A \int_{\tau} dt \mathbf{E}^{\text{ex}\circ}(\mathbf{r}_{\parallel}, z_{\text{ex}}, t) \cdot \partial_t \mathbf{P}^{\text{ex}\circ}(\mathbf{r}_{\parallel}, t). \quad (\text{C37})$$

Utilizing the Green's dyadic, Eq. (36) in the main paper, evaluated at $\mathbf{q}_{\parallel} = 0$ and the solution for $\mathbf{P}^{\text{ex}\circ}$, Eq. (62) in the main paper, yields

$$\mathbf{E}^{\text{ex}\circ}(\mathbf{r}_{\parallel}, z_{\text{ex}}, t) = \frac{\omega}{c} \frac{1}{2\varepsilon_0 \sqrt{\varepsilon_{\text{out}}}} \mathbf{P}^{\text{ex}\circ} \left(\mathbf{r}_{\parallel}, t - \frac{\pi}{2\omega} \right). \quad (\text{C38})$$

We insert the solution for $\mathbf{P}^{\text{ex}\circ}$, Eq. (62), as well as the parameter f_{o}^{ex} from table I in the main paper and evaluate the normalized exciton re-radiated energy, Eq. (C37), around the resonance ($\omega_{\text{ex}\circ} + \omega \approx 2\omega$). We find

$$w_{\text{rad}}^{\text{ex}\circ} = \frac{W_{\text{rad}}^{\text{ex}\circ}}{W^0} \approx -\frac{1}{2} \frac{(\gamma_{\text{o}}^{\text{ex}} - \gamma^{\text{ex}})(\gamma_{\text{o}}^{\text{ex}} - \gamma^{\text{ex}})}{|\omega - \omega_{\text{ex}\circ} + \frac{i}{2}\gamma_{\text{o}}^{\text{ex}}|^2}, \quad (\text{C39})$$

where $(\gamma_{\text{o}}^{\text{ex}} - \gamma^{\text{ex}})$ indicates solely the radiative losses. $w_{\text{rad}}^{\text{ex}\circ}$ is negative since it accounts for out-going energy.

For the MNP plasmon, the concept of splitting the extinction into absorption and re-radiated energy is similar. However, the explicit evaluation of the re-radiated energy $W_{\text{rad}}^{\text{pl}}$, that for the plasmon corresponds to scattering, gives rise to unphysical infinities. The reason is that the point-dipole approximation breaks down for the energy of the MNP plasmon in its own emitted electric field. However, we still observe the common proportionality of extinction to the square of the polarizability. A derivation of the scattering cross section of a small particle for the example of a dielectric sphere considering the geometry by a given polarizability is provided in Ref. 95. For the scope of this manuscript, we limit ourselves to the explicit evaluation of the radiative emission of the 2D excitons. This sufficiently serves as a proof of concept for assigning the both terms to their respective physical interpretations as re-radiated/scattered energy for bright exciton and MNP plasmon.

4. $W^0 = W_{\text{ext}}$: extinction

In the previous sections, we identified the radiated/scattered energy and proved that the contribution of the energy exchange to the energy balance vanish. Therefore, the extinction that is the only remaining term, equals the energy that the incident electric field loses on the system in the first place.

$$W_{\text{ext}} = W^0 = \int_{\tau} dt \int_V d^3r \mathbf{E}^0(\mathbf{r}, t) \cdot \dot{\mathbf{P}}(\mathbf{r}, t) \quad (\text{C40})$$

Here, it consists of three contributions

$$W_{\text{ext}}^{\text{pl}} = \int_{\tau} dt \int_V d^3r \mathbf{E}^0(\mathbf{r}, t) \cdot \partial_t \mathbf{P}^{\text{pl}}(\mathbf{r}, t), \quad (\text{C41})$$

$$W_{\text{ext}}^{\text{exo}} = \int_{\tau} dt \int_V d^3r \mathbf{E}^0(\mathbf{r}, t) \cdot \partial_t \mathbf{P}^{\text{exo}}(\mathbf{r}, t), \quad (\text{C42})$$

$$W_{\text{ext}}^{\text{ex}\bullet} = \int_{\tau} dt \int_V d^3r \mathbf{E}^0(\mathbf{r}, t) \cdot \partial_t \mathbf{P}^{\text{ex}\bullet}(\mathbf{r}, t). \quad (\text{C43})$$

First, we show that last term, $W_{\text{ext}}^{\text{ex}\bullet}$ vanishes since the incident electric field does not directly act on the dark-exciton dipole density. The thin film approximation, Eq. (C5), yields

$$W_{\text{ext}}^{\text{ex}\bullet} = \int_{\tau} dt \int_A d^2r_{\parallel} \mathbf{E}^0(\mathbf{r}_{\parallel}, z_{\text{ex}}, t) \cdot \partial_t \mathbf{P}^{\text{ex}\bullet}(\mathbf{r}_{\parallel}, t). \quad (\text{C44})$$

The considered incident electric field \mathbf{E}^0 is constant regarding the in-plane coordinate \mathbf{r}_{\parallel} . Therefore the \mathbf{r}_{\parallel} -integral can be treated as a Fourier transform of the $\text{ex}\bullet$ -dipole density, evaluated at $\mathbf{q}_{\parallel} = 0$. Since $\mathbf{P}_{\mathbf{q}_{\parallel}}^{\text{ex}\bullet}(t) = \mathbf{0}$, it follows

$$W_{\text{ext}}^{\text{ex}\bullet} = 0. \quad (\text{C45})$$

The full extinction is therefore given by the plasmon and bright exciton contribution

$$W_{\text{ext}} = W_{\text{ext}}^{\text{pl}} + W_{\text{ext}}^{\text{exo}}. \quad (\text{C46})$$

It is evaluated in the main paper, Eq. (71). To highlight the relation between extinction, absorption and radiative losses, we convert the result for the normalized exciton extinction $w_{\text{ext}}^{\text{ex}}$, Eq. (71) from the main paper, further. Around the resonance, where $\omega_{\text{exo}} + \omega \approx 2\omega$, we find

$$w_{\text{ext}}^{\text{ex}} \approx \frac{1}{2} \frac{(\gamma_{\circ}^{\text{ex}} - \gamma^{\text{ex}})\gamma_{\circ}^{\text{ex}}}{|\omega - \omega_{\text{exo}} + \frac{i}{2}\gamma_{\circ}^{\text{ex}}|^2}. \quad (\text{C47})$$

$(\gamma_{\circ}^{\text{ex}} - \gamma^{\text{ex}})$ indicates solely the radiative losses. Combining the normalized exciton radiated energy, Eq. (C39), and extinction, Eq. (C47), allows to determine the exciton absorption

$$w_{\text{abs}}^{\text{ex}} = w_{\text{ext}}^{\text{ex}} + w_{\text{rad}}^{\text{exo}} \approx \frac{1}{2} \frac{(\gamma_{\circ}^{\text{ex}} - \gamma^{\text{ex}})\gamma^{\text{ex}}}{|\omega - \omega_{\text{exo}} + \frac{i}{2}\gamma_{\circ}^{\text{ex}}|^2}. \quad (\text{C48})$$

This result confirms the allocation of the individual terms to extinction, radiated energy and absorption, since it matches the absorption that can be derived from the Elliot susceptibility for excitons, cp. e.g. Ref. 62.

Appendix D: Dependency on surrounding permittivity ε_{out}

To describe the MNP as a single effective harmonic oscillator, we had to neglect all absorption effects aside from the plasmonic absorption (intraband transitions in the metal conduction band). In particular, the absorption caused by interband transitions in the background permittivity ε_b is omitted that is the approximation $\text{Im}(\varepsilon_b) \approx 0$.

Fig. 8 illustrates the real and imaginary parts of the background permittivity (non-Drude) of gold, $\varepsilon_b(\omega)$, as defined in Eq. (20). The real part $\text{Re}(\varepsilon_b(\omega))$ (screening) dominates over the imaginary part $\text{Im}(\varepsilon_b(\omega))$ (absorption) in the range $\hbar\omega < 2.4$ eV, which limits the validity of our model to these energies, where interband transitions are negligible.

To test the validity of the approximation $\text{Im}(\varepsilon_b) \approx 0$, we compare the exact polarizability α that describes the electric field enhancement around the MNP with the approximated case where the absorption from interband transitions is neglected (i.e., setting $\text{Im}(\varepsilon_b) = 0$). Fig. 9 (left) shows the x -entry of the exact polarizability α_x , while the right panel depicts the simplified case without interband transition absorption. In our geometry, the y -entry of the polarizability is identical ($\alpha_y = \alpha_x$), and the z -entries not relevant, cp. Appendix B. This way, we assess the approximation for various surrounding permittivities $\varepsilon_{\text{out}} \in [1, 5]$.

The MNP's electric field enhancement, quantified by α_x , is a crucial ingredient to the exciton-plasmon coupling strength g_{eff} . The comparison reveals that the approximation ($\text{Im}(\varepsilon_b) = 0$), which is necessary to reduce the description of the MNP dynamics to a single oscillator model, gives rise to an inaccurate dependence on ε_{out} in the simplified coupling, table I. Specifically, for small $\varepsilon_{\text{out}} \approx 1$, the polarizability α_x is significantly overestimated, whereas for large $\varepsilon_{\text{out}} > 4$, it is underestimated. Furthermore, the MNP plasmon frequency moves outside the above mentioned allowed frequency range for $\varepsilon_{\text{out}} \lesssim 2$. This leads us to restrict the applicability of the derived coupling strength to $\varepsilon_{\text{out}} \in [2.5, 4.5]$. Within this range, we observe no significant dependence of the coupling strength g_{eff} on the surrounding permittivity ε_{out} . However, in agreement with the theories from Refs. [66, 94], the minimal field enhancement by the MNP, cp. Fig. 9 (left), at $\varepsilon_{\text{out}} \approx 1$ suggests that higher surrounding permittivities are necessary to reach the strong coupling regime.

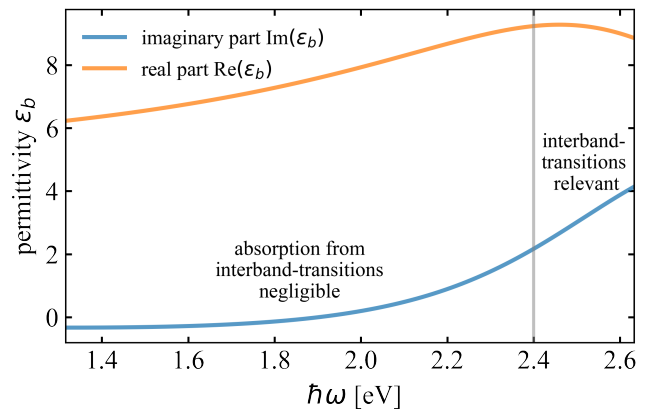


Figure 8. real and imaginary part of non-Drude permittivity ε_b of the MNP. The imaginary part corresponds to the absorption due to interband transitions. The real part incorporates screening due to inner shells. The approximation $\text{Im}(\varepsilon_b) \approx 0$ (corresponds to neglecting absorption from interband-transitions) is only valid for $\hbar\omega < 2.4$ eV (vertical line)

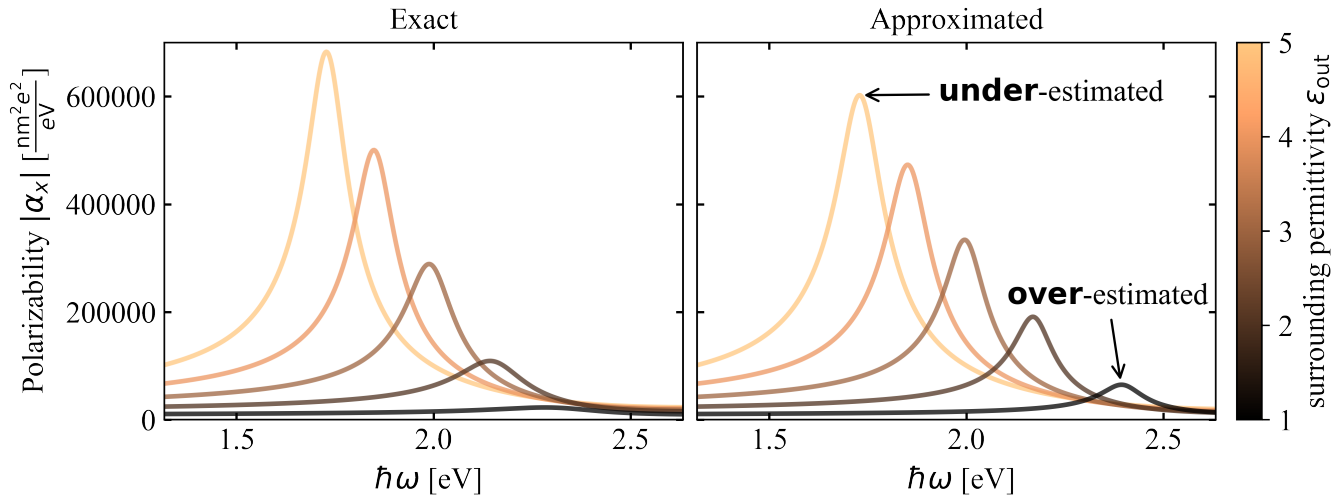


Figure 9. Comparison of exact MNP polarizability α_x (left) and the approximated α_x where $\text{Im}(\epsilon_b) \approx 0$ (right) for varying surrounding permittivity ϵ_{out} . The y -entries of the polarizability are identical; the z -entries here not relevant.

- [1] S. Yan, X. Zhu, J. Dong, Y. Ding, and S. Xiao, 2d materials integrated with metallic nanostructures: fundamentals and optoelectronic applications, *Nanophotonics* **9**, 1877 (2020).
- [2] A. J. Moilanen, T. K. Hakala, and P. Törmä, Active Control of Surface Plasmon–Emitter Strong Coupling, *ACS Photonics* **5**, 54 (2018).
- [3] T. Mahinroosta and S. Mehri Hamidi, Strong Exciton–Plasmon Coupling in Waveguide-Based Plexcitonic Nanostructures, *physica status solidi (b)* **257**, 2000266 (2020).
- [4] A. Salomon, S. Wang, J. A. Hutchison, C. Genet, and T. W. Ebbesen, Strong Light-Molecule Coupling on Plasmonic Arrays of Different Symmetry, *ChemPhysChem* **14**, 1882 (2013).
- [5] R. Chikkaraddy, B. de Nijs, F. Benz, S. J. Barrow, O. A. Scherman, E. Rosta, A. Demetriadou, P. Fox, O. Hess, and J. J. Baumberg, Single-molecule strong coupling at room temperature in plasmonic nanocavities, *Nature* **535**, 127 (2016).
- [6] M.-E. Kleemann, R. Chikkaraddy, E. M. Alexeev, D. Kos, C. Carnegie, W. Deacon, A. C. de Pury, C. Große, B. de Nijs, J. Mertens, A. I. Tartakovskii, and J. J. Baumberg, Strong-coupling of WSe₂ in ultra-compact plasmonic nanocavities at room temperature, *Nature Communications* **8**, 1296 (2017).
- [7] H. Leng, B. Szychowski, M.-C. Daniel, and M. Pelton, Strong coupling and induced transparency at room temperature with single quantum dots and gap plasmons, *Nature Communications* **9**, 4012 (2018).
- [8] H. Wei, X. Yan, Y. Niu, Q. Li, Z. Jia, and H. Xu, Plasmon–Exciton Interactions: Spontaneous Emission and Strong Coupling, *Advanced Functional Materials* **31**, 2100889 (2021).
- [9] S. Hu, J. Huang, R. Arul, A. Sánchez-Iglesias, Y. Xiong, L. M. Liz-Marzán, and J. J. Baumberg, Robust consistent single quantum dot strong coupling in plasmonic nanocavities, *Nature Communications* **15**, 6835 (2024).
- [10] D. E. Gómez, X. Shi, T. Oshikiri, A. Roberts, and H. Misawa, Near-Perfect Absorption of Light by Coherent Plasmon–Exciton States, *Nano Letters* **21**, 3864 (2021).
- [11] D. Melnikau, D. Savateeva, A. Susha, A. L. Rogach, and Y. P. Rakovich, Strong plasmon-exciton coupling in a hybrid system of gold nanostars and J-aggregates, *Nanoscale Research Letters* **8**, 134 (2013).
- [12] A. Raja, A. Chaves, J. Yu, G. Arefe, H. M. Hill, A. F. Rigosi, T. C. Berkelbach, P. Nagler, C. Schüller, T. Korn, C. Nuckolls, J. Hone, L. E. Brus, T. F. Heinz, D. R. Reichman, and A. Chernikov, Coulomb engineering of the bandgap and excitons in two-dimensional materials, *Nature Communications* **8**, 15251 (2017).
- [13] L. Greten, R. Salzwedel, M. Katzer, H. Mittenzwey, D. Christiansen, A. Knorr, and M. Selig, Dipolar Coupling at Interfaces of Ultrathin Semiconductors, Semimetals, Plasmonic Nanoparticles, and Molecules, *physica status solidi (a)* **221**, 2300102 (2024).
- [14] M. Feierabend, G. Berghäuser, A. Knorr, and E. Malic, Proposal for dark exciton based chemical sensors, *Nature Communications* **8**, 14776 (2017).
- [15] N. S. Mueller and S. Reich, Microscopic theory of optical absorption in graphene enhanced by lattices of plasmonic nanoparticles, *Physical Review B* **97**, 235417 (2018).
- [16] Z. Li, C. Liu, X. Rong, Y. Luo, H. Cheng, L. Zheng, F. Lin, B. Shen, Y. Gong, S. Zhang, and Z. Fang, Tailoring MoS₂ Valley-Polarized Photoluminescence with Super Chiral Near-Field, *Advanced Materials* **30**, 1801908 (2018).
- [17] Y. Xie, L. Yang, J. Du, and Z. Li, Giant Enhancement of Second-Harmonic Generation in Hybrid Metasurface Coupled MoS₂ with Fano-Resonance Effect, *Nanoscale Research Letters* **17**, 97 (2022).
- [18] T. Low, A. Chaves, J. D. Caldwell, A. Kumar, N. X. Fang, P. Avouris, T. F. Heinz, F. Guinea, L. Martin-Moreno, and F. Koppens, Polaritons in layered two-dimensional materials, *Nature Materials* **16**, 182 (2017).
- [19] P. Kusch, N. S. Mueller, M. T. Hartmann, and S. Reich, Strong light-matter coupling in MoS₂, *Physical Review B* **103**, 235409 (2021).
- [20] C. Schneider, M. M. Glazov, T. Korn, S. Höfling, and B. Ur-

- baszek, Two-dimensional semiconductors in the regime of strong light-matter coupling, *Nature Communications* **9**, 2695 (2018).
- [21] J. Kern, A. Trügler, I. Niehues, J. Ewering, R. Schmidt, R. Schneider, S. Najmaei, A. George, J. Zhang, J. Lou, U. Hohenester, S. Michaelis de Vasconcellos, and R. Bratschitsch, Nanoantenna-Enhanced Light-Matter Interaction in Atomically Thin WS₂, *ACS Photonics* **2**, 1260 (2015).
- [22] E. Palacios, S. Park, S. Butun, L. Lauhon, and K. Aydin, Enhanced radiative emission from monolayer MoS₂ films using a single plasmonic dimer nanoantenna, *Applied Physics Letters* **111**, 031101 (2017).
- [23] S. Butun, S. Tongay, and K. Aydin, Enhanced Light Emission from Large-Area Monolayer MoS₂ Using Plasmonic Nanodisc Arrays, *Nano Letters* **15**, 2700 (2015).
- [24] L. N. Tripathi, O. Iff, S. Betzold, L. Dusanowski, M. Emmerling, K. Moon, Y. J. Lee, S.-H. Kwon, S. Höfling, and C. Schneider, Spontaneous Emission Enhancement in Strain-Induced WSe₂ Monolayer-Based Quantum Light Sources on Metallic Surfaces, *ACS Photonics* **5**, 1919 (2018).
- [25] M. von Helversen, L. Greten, I. Limame, C.-W. Shih, P. Schlaugat, C. Antón-Solanas, C. Schneider, B. Rosal, A. Knorr, and S. Reitzenstein, Temperature dependent temporal coherence of metallic-nanoparticle-induced single-photon emitters in a WSe₂ monolayer, *2D Materials* **10**, 045034 (2023).
- [26] X. Xiong, N. Kongsuwan, Y. Lai, C. E. Png, L. Wu, and O. Hess, Room-temperature plexcitonic strong coupling: Ultrafast dynamics for quantum applications, *Applied Physics Letters* **118**, 130501 (2021).
- [27] A. Stefanu, N. J. Halas, P. Nordlander, and E. Cortes, Electronic excitations at the plasmon-molecule interface, *Nature Physics* **20**, 1065 (2024).
- [28] X. Li, J. Zhu, and B. Wei, Hybrid nanostructures of metal/two-dimensional nanomaterials for plasmon-enhanced applications, *Chem. Soc. Rev.* **45**, 3145 (2016).
- [29] H. Shan, Y. Yu, X. Wang, Y. Luo, S. Zu, B. Du, T. Han, B. Li, Y. Li, J. Wu, F. Lin, K. Shi, B. K. Tay, Z. Liu, X. Zhu, and Z. Fang, Direct observation of ultrafast plasmonic hot electron transfer in the strong coupling regime, *Light: Science & Applications* **8**, 9 (2019).
- [30] Z. Peng, T. W. Lo, and D. Lei, Plasmonic-hot-electron mediated room-temperature generation of charged biexciton in monolayer WS₂, *Physical Review Materials* **7**, 054002 (2023).
- [31] M. L. Brongersma, N. J. Halas, and P. Nordlander, Plasmon-induced hot carrier science and technology, *Nature Nanotechnology* **10**, 25 (2015).
- [32] X. Wu, S. K. Gray, and M. Pelton, Quantum-dot-induced transparency in a nanoscale plasmonic resonator, *Optics Express* **18**, 23633 (2010).
- [33] P. Törmä and W. L. Barnes, Strong coupling between surface plasmon polaritons and emitters: a review, *Reports on Progress in Physics* **78**, 013901 (2014).
- [34] M. F. Limonov, M. V. Rybin, A. N. Poddubny, and Y. S. Kivshar, Fano resonances in photonics, *Nature Photonics* **11**, 543 (2017).
- [35] Y. S. Joe, A. M. Satanin, and C. S. Kim, Classical analogy of Fano resonances, *Physica Scripta* **74**, 259 (2006).
- [36] M. O. Scully and M. S. Zubairy, *Quantum optics* (Cambridge university press, 1997).
- [37] T. Wu, C. Wang, G. Hu, Z. Wang, J. Zhao, Z. Wang, K. Chaykun, L. Liu, M. Chen, D. Li, S. Zhu, Q. Xiong, Z. Shen, H. Gao, F. J. Garcia-Vidal, L. Wei, Q. J. Wang, and Y. Luo, Ultrastrong exciton-plasmon couplings in WS₂ multilayers synthesized with a random multi-singular metasurface at room temperature, *Nature Communications* **15**, 3295 (2024).
- [38] N. S. Mueller, Y. Okamura, B. G. M. Vieira, S. Juergensen, H. Lange, E. B. Barros, F. Schulz, and S. Reich, Deep strong light-matter coupling in plasmonic nanoparticle crystals, *Nature* **583**, 780 (2020).
- [39] S. Hughes, C. Gustin, and F. Nori, Reconciling quantum and classical spectral theories of ultrastrong coupling: role of cavity bath coupling and gauge corrections, *Optica Quantum* **2**, 133 (2024).
- [40] P. Forn-Díaz, L. Lamata, E. Rico, J. Kono, and E. Solano, Ultrastrong coupling regimes of light-matter interaction, *Reviews of Modern Physics* **91**, 025005 (2019).
- [41] A. Frisk Kockum, A. Miranowicz, S. De Liberato, S. Savasta, and F. Nori, Ultrastrong coupling between light and matter, *Nature Reviews Physics* **1**, 19 (2019).
- [42] F. Todisco, S. D'Agostino, M. Esposito, A. I. Fernández-Domínguez, M. De Giorgi, D. Ballarini, L. Dominici, I. Tarantini, M. Cuscuná, F. Della Sala, G. Gigli, and D. Sanvitto, Exciton-Plasmon Coupling Enhancement via Metal Oxidation, *ACS Nano* **9**, 9691 (2015).
- [43] W. Wang, P. Vasa, R. Pomraenke, R. Vogelgesang, A. De Sio, E. Sommer, M. Maiuri, C. Manzoni, G. Cerullo, and C. Lienau, Interplay between Strong Coupling and Radiative Damping of Excitons and Surface Plasmon Polaritons in Hybrid Nanostructures, *ACS Nano* **8**, 1056 (2014).
- [44] F. Wu, J. Guo, Y. Huang, K. Liang, L. Jin, J. Li, X. Deng, R. Jiao, Y. Liu, J. Zhang, W. Zhang, and L. Yu, Plexcitonic Optical Chirality: Strong Exciton-Plasmon Coupling in Chiral J-Aggregate-Metal Nanoparticle Complexes, *ACS Nano* **15**, 2292 (2021).
- [45] F. Todisco, M. De Giorgi, M. Esposito, L. De Marco, A. Zizzari, M. Bianco, L. Dominici, D. Ballarini, V. Arima, G. Gigli, and D. Sanvitto, Ultrastrong Plasmon-Exciton Coupling by Dynamic Molecular Aggregation, *ACS Photonics* **5**, 143 (2018).
- [46] I. Abid, W. Chen, J. Yuan, A. Bohloul, S. Najmaei, C. Avendano, R. Péchou, A. Mlayah, and J. Lou, Temperature-Dependent Plasmon-Exciton Interactions in Hybrid Au/MoSe₂ Nanostructures, *ACS Photonics* **4**, 1653 (2017).
- [47] A. Bisht, J. Cuadra, M. Wersäll, A. Canales, T. J. Antosiewicz, and T. Shegai, Collective Strong Light-Matter Coupling in Hierarchical Microcavity-Plasmon-Exciton Systems, *Nano Letters* **19**, 189 (2019).
- [48] B. Lee, W. Liu, C. H. Naylor, J. Park, S. C. Malek, J. S. Berger, A. T. C. Johnson, and R. Agarwal, Electrical Tuning of Exciton-Plasmon Polariton Coupling in Monolayer MoS₂ Integrated with Plasmonic Nanoantenna Lattice, *Nano Letters* **17**, 4541 (2017).
- [49] M. Zhang, Y. Tian, X. Chen, Z. Sun, X. Zhu, and J. Wu, Observation of ultra-large Rabi splitting in the plasmon-exciton polaritons at room temperature, *Nanophotonics* **12**, 3267 (2023).
- [50] I. Abid, A. Bohloul, S. Najmaei, C. Avendano, H.-L. Liu, R. Péchou, A. Mlayah, and J. Lou, Resonant surface plasmon-exciton interaction in hybrid MoSe₂@Au nanostructures, *Nanoscale* **8**, 8151 (2016).
- [51] W. Liu, B. Lee, C. H. Naylor, H.-S. Ee, J. Park, A. T. C. Johnson, and R. Agarwal, Strong Exciton-Plasmon Coupling in MoS₂ Coupled with Plasmonic Lattice, *Nano Letters* **16**, 1262 (2016).
- [52] S. Wang, S. Li, T. Chervy, A. Shalabney, S. Azzini, E. Orgiu, J. A. Hutchison, C. Genet, P. Samorì, and T. W. Ebbesen, Co-

- herent Coupling of WS₂ Monolayers with Metallic Photonic Nanostructures at Room Temperature, *Nano Letters* **16**, 4368 (2016).
- [53] Y. Zhu, J. Yang, J. Abad-Arredondo, A. I. Fernández-Domínguez, F. J. Garcia-Vidal, and D. Natelson, Electroluminescence as a probe of strong exciton–plasmon coupling in few-layer WSe₂, *Nano Letters* **24**, 525 (2024).
- [54] M. M. Petrić, M. Kremser, M. Barbone, A. Nolinder, A. Lyamkina, A. V. Stier, M. Kaniber, K. Müller, and J. J. Finley, Tuning the Optical Properties of a MoSe₂ Monolayer Using Nanoscale Plasmonic Antennas, *Nano Letters* **22**, 561 (2022).
- [55] D. Zheng, S. Zhang, Q. Deng, M. Kang, P. Nordlander, and H. Xu, Manipulating Coherent Plasmon–Exciton Interaction in a Single Silver Nanorod on Monolayer WSe₂, *Nano Letters* **17**, 3809 (2017).
- [56] J. Cuadra, D. G. Baranov, M. Wersäll, R. Verre, T. J. Antosiewicz, and T. Shegai, Observation of Tunable Charged Exciton Polaritons in Hybrid Monolayer WS₂ - Plasmonic Nanoantenna System, *Nano Letters* **18**, 1777 (2018).
- [57] M. Geisler, X. Cui, J. Wang, T. Rindzevicius, L. Gammelgaard, B. S. Jessen, P. A. D. Gonçalves, F. Todisco, P. Bøggild, A. Boisen, M. Wubs, N. A. Mortensen, S. Xiao, and N. Stenger, Single-Crystalline Gold Nanodisks on WS₂ Mono- and Multilayers for Strong Coupling at Room Temperature, *ACS Photonics* **6**, 994 (2019).
- [58] J. Qin, Y.-H. Chen, Z. Zhang, Y. Zhang, R. J. Blaikie, B. Ding, and M. Qiu, Revealing Strong Plasmon-Exciton Coupling between Nanogap Resonators and Two-Dimensional Semiconductors at Ambient Conditions, *Physical Review Letters* **124**, 063902 (2020).
- [59] J. Wen, H. Wang, W. Wang, Z. Deng, C. Zhuang, Y. Zhang, F. Liu, J. She, J. Chen, H. Chen, S. Deng, and N. Xu, Room-Temperature Strong Light–Matter Interaction with Active Control in Single Plasmonic Nanorod Coupled with Two-Dimensional Atomic Crystals, *Nano Letters* **17**, 4689 (2017).
- [60] B. Lee, J. Park, G. H. Han, H.-S. Ee, C. H. Naylor, W. Liu, A. C. Johnson, and R. Agarwal, Fano Resonance and Spectrally Modified Photoluminescence Enhancement in Monolayer MoS₂ Integrated with Plasmonic Nanoantenna Array, *Nano Letters* **15**, 3646 (2015).
- [61] T. Pincelli, T. Vasileiadis, S. Dong, S. Beaulieu, M. Dendzik, D. Zahn, S.-E. Lee, H. Seiler, Y. Qi, R. P. Xian, J. Maklar, E. Coy, N. S. Mueller, Y. Okamura, S. Reich, M. Wolf, L. Rettig, and R. Ernstorfer, Observation of Multi-Directional Energy Transfer in a Hybrid Plasmonic–Excitonic Nanostructure, *Advanced Materials* **35**, 2209100 (2023).
- [62] M. Kira and S. W. Koch, *Semiconductor quantum optics* (Cambridge University Press, Cambridge ; New York, 2012).
- [63] G. Mie, Beiträge zur Optik trüber Medien, speziell kolloidaler Metallösungen, *Annalen der Physik* **330**, 377 (1908).
- [64] R. Gans, Über die Form ultramikroskopischer Goldteilchen, *Annalen der Physik* **342**, 881 (1912).
- [65] C. F. Bohren and D. R. Huffman, *Absorption and scattering of light by small particles* (Wiley, New York, 1983).
- [66] L. Greten, R. Salzwedel, T. Göde, D. Greten, S. Reich, S. Hughes, M. Selig, and A. Knorr, Strong Coupling of Two-Dimensional Excitons and Plasmonic Photonic Crystals: Microscopic Theory Reveals Triplet Spectra, *ACS Photonics* **11**, 1396 (2024).
- [67] G. Wang, A. Chernikov, M. M. Glazov, T. F. Heinz, X. Marie, T. Amand, and B. Urbaszek, *Colloquium: Excitons in atomically thin transition metal dichalcogenides*, *Reviews of Modern Physics* **90**, 021001 (2018).
- [68] A. Knorr, S. Hughes, T. Stroucken, and S. Koch, Theory of ultrafast spatio-temporal dynamics in semiconductor heterostructures, *Chemical Physics* **210**, 27 (1996).
- [69] M. Selig, F. Katsch, R. Schmidt, S. Michaelis de Vasconcellos, R. Bratschitsch, E. Malic, and A. Knorr, Ultrafast dynamics in monolayer transition metal dichalcogenides: Interplay of dark excitons, phonons, and intervalley exchange, *Physical Review Research* **1**, 022007 (2019).
- [70] A. Kormányos, G. Burkard, M. Gmitra, J. Fabian, V. Zólyomi, N. D. Drummond, and V. Fal’ko, **k · p** theory for two-dimensional transition metal dichalcogenide semiconductors, *2D Materials* **2**, 022001 (2015).
- [71] M. Selig, G. Berghäuser, M. Richter, R. Bratschitsch, A. Knorr, and E. Malic, Dark and bright exciton formation, thermalization, and photoluminescence in monolayer transition metal dichalcogenides, *2D Materials* **5**, 035017 (2018).
- [72] M. Katzer, S. Kovalchuk, K. Greben, K. I. Bolotin, M. Selig, and A. Knorr, Impact of dark excitons on Förster-type resonant energy transfer between dye molecules and atomically thin semiconductors, *Physical Review B* **107**, 035304 (2023).
- [73] M. Selig, G. Berghäuser, A. Raja, P. Nagler, C. Schüller, T. F. Heinz, T. Korn, A. Chernikov, E. Malic, and A. Knorr, Excitonic linewidth and coherence lifetime in monolayer transition metal dichalcogenides, *Nature Communications* **7**, 13279 (2016).
- [74] G. Berghäuser and E. Malic, Analytical approach to excitonic properties of MoS₂, *Physical Review B* **89**, 125309 (2014).
- [75] D. Xiao, G.-B. Liu, W. Feng, X. Xu, and W. Yao, Coupled Spin and Valley Physics in Monolayers of MoS₂ and Other Group-VI Dichalcogenides, *Physical Review Letters* **108**, 196802 (2012).
- [76] H. Haug and S. W. Koch, *Quantum theory of the optical and electronic properties of semiconductors*, 4th ed. (World Scientific, Singapore ; River Edge, NJ, 2004).
- [77] M. Schubert and B. Wilhelmi, *Nonlinear optics and quantum electronics* (1986).
- [78] A. O. Slobodeniuk and D. M. Basko, Spin-flip processes and radiative decay of dark intravalley excitons in transition metal dichalcogenide monolayers, *2D Materials* **3**, 035009 (2016).
- [79] G. Wang, C. Robert, M. M. Glazov, F. Cadiz, E. Courtade, T. Amand, D. Lagarde, T. Taniguchi, K. Watanabe, B. Urbaszek, and X. Marie, In-Plane Propagation of Light in Transition Metal Dichalcogenide Monolayers: Optical Selection Rules, *Physical Review Letters* **119**, 047401 (2017).
- [80] Y. Zhou, G. Scuri, D. S. Wild, A. A. High, A. Dibos, L. A. Jauregui, C. Shu, K. De Greve, K. Pistunova, A. Y. Joe, T. Taniguchi, K. Watanabe, P. Kim, M. D. Lukin, and H. Park, Probing dark excitons in atomically thin semiconductors via near-field coupling to surface plasmon polaritons, *Nature Nanotechnology* **12**, 856 (2017).
- [81] L. Landau, On the vibrations of the electronic plasma, *Zhurnal eksperimentalnoi i teoreticheskoi fiziki* **16**, 574 (1946).
- [82] P. Drude, Zur Elektronentheorie der Metalle, *Annalen der Physik* **306**, 566 (1900).
- [83] H. Wang, F. Tam, N. K. Grady, and N. J. Halas, Cu Nanoshells: Effects of Interband Transitions on the Nanoparticle Plasmon Resonance, *The Journal of Physical Chemistry B* **109**, 18218 (2005).
- [84] A. Vial, A.-S. Grimault, D. Macías, D. Barchiesi, and M. L. de la Chapelle, Improved analytical fit of gold dispersion: Application to the modeling of extinction spectra with a finite-difference time-domain method, *Phys. Rev. B* **71**, 085416 (2005).
- [85] P. G. Etchegoin, E. C. Le Ru, and M. Meyer, An analytic

- model for the optical properties of gold, *The Journal of Chemical Physics* **125**, 164705 (2006).
- [86] V. Myroshnychenko, J. Rodríguez-Fernández, I. Pastoriza-Santos, A. M. Funston, C. Novo, P. Mulvaney, L. M. Liz-Marzán, and F. J. García de Abajo, Modelling the optical response of gold nanoparticles, *Chemical Society Reviews* **37**, 1792 (2008).
- [87] U. Kreibig and M. Vollmer, *Optical properties of metal clusters*, Vol. 25 (Springer Science & Business Media, 2013).
- [88] P. B. Johnson and R. W. Christy, Optical Constants of the Noble Metals, *Physical Review B* **6**, 4370 (1972).
- [89] E. D. Palik, *Handbook of optical constants of solids*, Vol. 3 (Academic press, 1998).
- [90] M. Liu, M. Pelton, and P. Guyot-Sionnest, Reduced damping of surface plasmons at low temperatures, *Physical Review B* **79**, 035418 (2009).
- [91] J. A. McKay and J. A. Rayne, Temperature dependence of the infrared absorptivity of the noble metals, *Physical Review B* **13**, 673 (1976).
- [92] G. R. Parkins, W. E. Lawrence, and R. W. Christy, Intra-band optical conductivity of Cu, Ag, and Au: Contribution from electron-electron scattering, *Physical Review B* **23**, 6408 (1981).
- [93] J.-S. G. Bouillard, W. Dickson, D. P. O'Connor, G. A. Wurtz, and A. V. Zayats, Low-Temperature Plasmonics of Metallic Nanostructures, *Nano Letters* **12**, 1561 (2012).
- [94] R. Salzwedel, L. Greten, S. Schmidt, S. Hughes, A. Knorr, and M. Selig, Spatial exciton localization at interfaces of metal nanoparticles and atomically thin semiconductors, *Phys. Rev. B* **109**, 035309 (2024).
- [95] J. D. Jackson, *Classical electrodynamics* (John Wiley & Sons, 2021).
- [96] D. Y. Qiu, T. Cao, and S. G. Louie, Nonanalyticity, Valley Quantum Phases, and Lightlike Exciton Dispersion in Monolayer Transition Metal Dichalcogenides: Theory and First-Principles Calculations, *Physical Review Letters* **115**, 176801 (2015).
- [97] M. M. Glazov and R. A. Suris, Ultrafast exciton transport in van der Waals heterostructures (2024), arXiv:2403.19571 [cond-mat].
- [98] J.-Y. Yan, W. Zhang, S. Duan, X.-G. Zhao, and A. O. Govorov, Optical properties of coupled metal-semiconductor and metal-molecule nanocrystal complexes: Role of multipole effects, *Phys. Rev. B* **77**, 165301 (2008).
- [99] R. S. Swathi and K. L. Sebastian, Distance dependence of fluorescence resonance energy transfer, *Journal of Chemical Sciences* **121**, 777 (2009).
- [100] P. A. D. Gonçalves, L. P. Bertelsen, S. Xiao, and N. A. Mortensen, Plasmon-exciton polaritons in two-dimensional semiconductor/metal interfaces, *Physical Review B* **97**, 041402 (2018).
- [101] S. Vadia, J. Scherzer, K. Watanabe, T. Taniguchi, and A. Högele, Magneto-Optical Chirality in a Coherently Coupled Exciton-Plasmon System, *Nano Letters* **23**, 614 (2023).
- [102] W. Zhang, J.-B. You, J. Liu, X. Xiong, Z. Li, C. E. Png, L. Wu, C.-W. Qiu, and Z.-K. Zhou, Steering Room-Temperature Plexcitonic Strong Coupling: A Diexcitonic Perspective, *Nano Letters* **21**, 8979 (2021).
- [103] L. Hou, Q. Wang, H. Zhang, P. Wang, X. Gan, F. Xiao, and J. Zhao, Simultaneous control of plasmon-exciton and plasmon-trion couplings in an Au nanosphere and monolayer WS₂ hybrid system, *APL Photonics* **7**, 026107 (2022).
- [104] N. S. Rytova, Screened potential of a point charge in a thin film, *Moscow University Physics Bulletin* **3** (1967).
- [105] L. V. Keldysh, Coulomb interaction in thin semiconductor and semimetal films, *JETP Letters* **29**, 658 (1979).
- [106] E. B. Barros, B. G. Vieira, N. S. Mueller, and S. Reich, Plasmon-Polaritons in Nanoparticle Supercrystals: Microscopic Quantum Theory Beyond the Dipole Approximation, *Physical Review B* **104**, 035403 (2021).
- [107] M. V. Gurrieri, E. V. Denning, K. Seegert, P. T. Kristensen, and J. Mørk, Dynamics and condensation of polaritons in an optical nanocavity coupled to two-dimensional materials, *Physical Review B* **109**, 155432 (2024).
- [108] E. V. Denning, M. Wubs, N. Stenger, J. Mørk, and P. T. Kristensen, Quantum theory of two-dimensional materials coupled to electromagnetic resonators, *Physical Review B* **105**, 085306 (2022).